Glycoengineered keratinocyte library reveals essential functions of specific glycans for all stages of HSV-1 life cycle

Running title: Different classes of glycans are essential for all stages of HSV-1 life cycle

Ieva Bagdonaite[1]*, Irina N Marinova[1], Asha M Rudjord-Levann[1], Emil MH Pallesen[1], Sarah King-Smith[1], Troels B Rømer[1], Yen-Hsi Chen[1], Sally Dabelsteen[2] and Hans H Wandall[1]*

[1] Copenhagen Center for Glycomics, Institute of Cellular and Molecular Medicine, University of Copenhagen, DK-2200 Copenhagen, Denmark

[2] School of Dentistry, University of Copenhagen, DK-2200 Copenhagen, Denmark

* Corresponding authors

E-mail: hhw@sund.ku.dk (HHW) and ieva@sund.ku.dk (IB)

Abstract

Enveloped viruses encounter multiple types of cellular glycans throughout their infectious cycles, eventually acquiring surface glycans themselves, largely determined by the cellular glycosyltransferase and modifying enzyme repertoire. The cellular glycans have the potential for modulating virus-host interactions, whereas the acquired glycans are expected to have broad functional and immunological implications with importance for the diagnosis and treatment of viral infections. Still, we only have limited tools to dissect the role of the individual classes of glycans in viral biology in a meaningful context. We have recently introduced genetic engineering as a powerful tool to dissect the importance of glycosylation in cell biology. Here we generated a glycoengineered cell library in human keratinocytes by CRISPR/Cas9 and ZFN gene editing composed of cells lacking different glycosyltransferases delineating human glycosylation pathways, and used it to address the importance of glycans in a clinically relevant model for herpes simplex virus type 1 (HSV-1).

We propagated HSV-1 in cell lines with perturbations in the major classes of glycan structures, affecting the elongation and branching of N-linked and O-linked glycans, as well as elongation of glycosaminoglycans and glycosphingolipids. We also investigated the impact of site-specific O-glycosylation on the function of indispensable HSV-1 glycoproteins gB and gD. We find that distinct glycan structures are important at different stages of the virus life cycle; attachment, entry, and spread in the mutant cell lines as well as 3D organotypic skin equivalents. Our results show the importance of cellular glycosaminoglycans and glycolipids for attachment of HSV-1, N-glycans for entry and spread, and O-glycans for propagation. We further show that global changes in all elongated glycan structures of infection-competent virions had minimal effects on the early interactions with wild type cells. In contrast mutation of Ser or Thr residues at specific O-glycosylation sites directly affected glycoprotein surface expression and function. In conclusion, the data demonstrates the utility of genetic engineering to elucidate the roles of specific viral and cellular carbohydrate structures in herpesvirus biology. The method is applicable to other viral systems. The work also suggests close adaptation of HSV-1 to the cellular glycome while ensuring limited dependance on viral surface glycan structures for survival.

Introduction

Upon infection of human cells with enveloped viruses, the virus hijacks our secretory pathway leading to the decoration of the newly formed viral proteins and membranes with host glycans. The resulting glycans influence several aspects of viral biology, with the most appreciated function being immunological shields that prevent our immune system to recognize the viral particles [1]. However, many more functions are expected to be mediated by cellular and viral glycans, such as viral tropism, the clinical course of viral infections, and envelope glycoprotein function. Nevertheless, the abundantly present glycans are still underexplored as targets in new interventions used for treatments or in the design of new vaccines. The main obstacles to achieve such functional insights is the lack an accessible human model system that allows the systematic analysis of the contribution of distinct glycan structures.

Glycosylation is among the most complex and diverse post-translational modifications dynamically shaping the glycans on cellular proteins and lipids traveling through the secretory pathway and comprising an extensive glycocalyx on the cell surface. There are three major classes of cell surface glycoconjugates – glycoproteins, glycosphingolipids and proteoglycans carrying long glycosaminoglycan (GAG) chains – that all carry out numerous functions in human cells, including fine-tuning of molecular interactions, cell communication and immune modulation [2-4]. Due to non-template driven synthesis of glycans and the resulting heterogeneity it is challenging to investigate the functions of specific glycans in biological systems, let alone introducing an additional layer of complexity of viral infection. We have recently introduced genetic engineering to dissect the importance of glycosylation in cell and molecular biology, and generated glycoengineered cell libraries by CRISPR/Cas9 gene editing composed of cells lacking different glycosyltransferases delineating human glycosylation pathways [5-8].

Here we used the highly prevalent herpes simplex virus type 1 (HSV-1) as a relevant model to systematically assess the importance of specific glycans in infection of a relevant human cellular system; the human skin. We built a library of glycoengineered HaCaT keratinocytes by introducing targeted alterations in the cellular glycome, including select initiation, branching and capping events, and encompassing all the major classes of glycocojungates. The use of live virus in a natural target cell type, representing the primary site of infection, allowed us both to examine

isolated viral life cycle events using cultured cells, as well as follow viral spread in 3D differentiated skin tissue models built with the glycoengineered cells.

HSV-1 is a widespread human pathogen persisting in the neurons for a lifetime and causing recurrent cutaneous lesions due to reactivation [9]. Importantly, it can cause life-threatening CNS complications, which is a major risk for immunocompromised individuals, and predispose to neurodegenerative disease [10-12]. HSV-1 is a large dsDNA enveloped virus, encoding 12 surface glycoproteins important for viral entry, particle formation, and cell-to-cell spread [13, 14]. Cell and viral surface glycans are attached and assembled in the secretory pathway – the ER and the Golgi apparatus, which are hijacked by HSV-1 for secretion of viral proteins that acquire host-like glycosylation. The most abundant of those are N-linked glycans, essential for protein folding, and mucin type O-linked glycans. HSV-1 is known to possess both of these classes of glycans, and we have previously demonstrated the importance of elongated O-linked glycans for HSV-1 propagation [15-18]. On the cellular side, HSV-1 can interact with several different receptors for attachment and entry using distinct sets of viral proteins. This includes nectin-1, herpes virus entry mediator (HVEM), 3-O-sulfated heparan sulfate, integrins, as well as paired immunoglobulin-like receptor alpha (PILRα), which can be engaged by gD, gB or gH/gL [19-23]. Thus, it is conceivable that glycans on both the specific cellular receptors and the viral envelope proteins may play a role in the distinct interactions. Furthermore, the importance of GAGs for HSV-1 initial attachment is well documented [24, 25], while little is known about the role of glycosphingolipids.

We here generated a glycoengineered cell (2D) and tissue (3D) libraries in the human keratinocyte cell line, HaCaT, toinvestigate the yet unknown functions of distinct glycan structures, including various N-glycans, mucin type O-glycans, glycosaminoglycans, and glycosphingolipids on HSV-1 life cycle. We find that each individual glycan class affects at least one stage of HSV-1 life cycle – attachment, entry, propagation, or spread – in a natural human host cell type upon productive infection. We furthermore addressed roles of specific O-glycan acceptor amino acids on viral entry receptor gD and conserved fusogen gB. The work identifies the glycosylation steps that are essential for proper viral functions defining the scope of future mechanistic studies. The findings also suggest that local targeting of host glycosylation pathways by inhibitors or mimetics may inhibit redundant viral entry mechanisms.

Results

Generation of a glycogene knock out library in HaCaT keratinocytes

HaCaT keratinocytes represent a natural target organ for HSV-1 and are also capable of forming a stratified squamous epithelium, allowing to evaluate HSV-1 spread characteristics in tissue.

In order to address the role of different glycan structures in HSV-1 biology, we generated a library of genetically engineered cells delineating defined glycosylation pathways, including N-linked glycosylation and mucin type O-linked glycosylation, as well as glycosphingolipid and glycosaminoglycan synthesis. We used CRISPR/Cas9 technology coupled to lentiviral transduction or ZFN targeting followed by limited dilution cloning to generate stable knock outs (KO) of glycogenes of interest, and validated the library by indel amplicon analysis (IDAA) and Sanger sequencing (Figure 1A, Table S1). We targeted glycosyltransferases involved in the early stages of core structure synthesis, as well as major elongation and branching steps. We performed MS-based glycoprofiling to evaluate changes in N- and O-linked glycan structures. N-glycoprofiling revealed that wild type HaCaT keratinocytes presented with bi-, tri-, and tetra-antennary complex N-glycan structures with various degrees of sialylation, as well as high mannose type N-glycans (Figure 1B). In addition, CORA-based O-glycoprofiling has shown predominantly core 1 and core 2 type O-linked glycans (Figure 1C).

For N-linked glycans we generated *MGAT1*, *MGAT4A*, *MGAT4B*, *MGAT5*, and *MGAT5+4B* knock outs. MGAT1 adds the first N-acetylglucosamine to the C-2 of core α3-linked mannose, and lack of this enzyme results in elimination of all N-glycan maturation steps, yielding high-mannose type N-glycans (Figure 1A, 1B). MGAT4A, MGAT4B and MGAT5 are responsible for N-glycan branching, where MGAT4A or MGAT4B initiate a β4-linked antenna on the α3-linked mannose, and MGAT5 performs β6-linked branching from the core α6-linked mannose. Lack of MGAT5 should thus result in loss of tetra-antennary N-glycans, whereas loss of MGAT4A or MGAT4B isoforms would contribute to reduction in tetra-antennary N-glycan content (Figure 1A). Practically, the low-abundance tetra-antennary glycans were not detectable in knock out cells of either of the three branching enzymes, and other changes in complex N-glycan abundance distribution were observed (Figure 1B).

For mucin type O-linked glycans, we knocked out core 1 synthase (*C1GALT1*), its obligate chaperone COSMC (*C1GALT1C1*), core 2 synthase (*GCNT1*), as well as the major core 1-capping glycosyltransferase *ST3GAL1*. Loss of C1GALT1 or COSMC eliminates the β3-linked galactose (core 1 structure) and results in truncation of O-linked glycans to the initiating α-GalNAc (with and without α6 sialylation), whereas loss of GCNT1 abolishes the subsequent addition of β6-linked GlcNAc (core 2 structure), eliminating O-glycan branching (Figure 1A, 1C). Some structures matching the composition of monosialylated core 2 structures could still be detected, though they cannot be discriminated from core 1 structures matching the same composition. Finally, loss of ST3GAL1 significantly reduces the α3-linked sialic acid content and results in predominantly non-capped core 1 structures (Figure 1A, 1C).

We also targeted synthesis of glycosphingolipids and glycosaminoglycans (GAGs). Through knock out of *B4GALT5* or *ST3GAL5*, which represent non-redundant steps of GM3 glycosphingolipid synthesis, we generated cells with the truncated glycosphingolipids, glucosylceramide (GlcCer) and lactosylceramide (LacCer), respectively. Furthermore, we knocked out *B4GALT7*, which adds a β4-linked galactose to the initiating xylose in GAG biosynthesis, effectively truncating all classes of GAGs on membrane proteoglycans.

The generated keratinocyte library represents a screening platform for roles of defined cell-surface presented glycan structures in HSV-1 biology in the context of natural infection and with minimal perturbations of the total cellular glycome.

Propagation of HSV-1 in glycoengineered keratinocytes

In order to estimate the capacity of HSV-1 to replicate in glycoengineered keratinocytes, we infected confluent monolayers of the knock out cell lines with MOI 10 of HSV-1, and quantified the total and infectious particles in the media at 17 hpi by qPCR and plaque titration on GMK cells, respectively. We then calculated the total/infectious particle ratios for each knock out to evaluate viral replication fitness. HSV-1 could replicate in all the investigated cell lines, however, markedly decreased titers were detected in the media from *C1GALT1* and *C1GALT1C1* knock outs, leading to O-linked glycan truncation (Figure 1D). In contrast, close to normal levels of total particles were generated (Figure 1E), suggesting decreased fitness of virions lacking elongated O-glycans.

Somewhat lower numbers of infectious particles were produced in cells lacking N-glycan maturation (*MGAT1* KO), which was also reflected in an increased total/infectious particle ratio (Figure 1F), suggesting importance of complex N-linked glycans for viral fitness. Interestingly, decreased total/infectious particle ratios were observed in cell lines lacking the β6-antennae on N-glycans (*MGAT5*, *MGAT5+4B*), suggesting a higher proportion of progeny virions were infectious. A trend towards accelerated production of viral particles was identified for cells deficient in O-glycan sialylation (*ST3GAL1 KO*), glycosphingolipid sialylation (*ST3GAL5* KO) and GAG synthesis (*B4GALT7* KO). While virions generated in *ST3GAL1 KO* and *ST3GAL5* KO keratinocytes exhibited normal fitness characteristics, a lower percentage of *B4GALT7* KO generated virions were infectious (Figure 1F). In conclusion, apart from significant loss of titers in cells bearing truncated O-glycans, most of the tested disruptions in human glycosylation pathways permitted HSV-1 replication. We next investigated the major steps of HSV-1 infectious cycle to evaluate the individual contributions of defined glycan classes to early virus-cell interactions, viral particle formation, properties of glycoengineered virions and cell-to-cell spread.

Binding and entry of HSV-1 to mutant cell lines

We addressed the role of host cell glycans on early virus-cell interactions by testing the wild type virus binding and entry to the suite of mutant cell lines. HSV-1 is able to bind and enter human keratinocytes very rapidly, with around 30 % of virions bound after 20 min on ice, 80 % after 2 hours and complete binding after 3 hours. Furthermore, most of the bound virions enter keratinocytes within 5 min after warming [26]. To assess viral binding, we allowed for 200 PFU of HSV-1 to adsorb to cell monolayers on ice for 20 min or 120 min, followed by washing off unbound virions. For entry experiments, after 120 min on ice the plates were washed and moved to 37 °C for 5 min, followed by acid inactivation of non-entered virions.

Most of the tested classes of glycoconjugates were involved in early virus to cell interactions, and similar effects were observed both at 20 and 120 min on ice (Figure 2A-C). Glycolipid truncation to both LacCer and GlcCer adversely affected viral binding to around 50 % of that of WT (Figure 2A, 2B). Reduction of binding was also observed to cells with immature N-glycans (*MGAT1* KO) and those with reduced β4-antenna branching (*MGAT4B* KO), as well as those with reduced core 1 O-

glycan sialylation (*ST3GAL1* KO). In contrast, lack of core 2 O-glycan branching resulted in increased attachment (Figure 2A, 2B). The effects observed for binding were also reflected in the subsequent entry experiments (Figure 2D, 2E). Interestingly, *MGAT4A* KO, another isoform catalysing N-glycan β4-antenna synthesis in host cells, selectively affected viral entry, but not attachment (Figure 2E). This could signify the proposed different preferences of host protein substrates by the two isoenzymes, as well as unequal contribution to the overall glycoprofile [27]. In addition, an incremental reduction in entry was observed for *B4GALT5* KO cells, suggesting involvement of glycolipids in both viral binding and entry to host cells (Figure 2D, 2E). Finally, GAG synthesis was essential for viral attachment, and very few plaques were detected even after 2 hours on ice, which fits well with the known importance of heparan sulfate (HS) in the initial attachment of HSV-1 (Figure 2A, 2B) [24]. In conclusion, perturbations in the cellular glycome landscape have immediate effects to early virus-cell interactions.

To investigate the GAG binding determinants in more detail we performed two types of experiments using recombinant HSV-1 gC, which can bind both HS and chondroitin sulfate (CS) *in vitro*, similarly to intact HSV-1 [25, 28, 29]. Treatment of HaCaT WT cells with heparinases 1, 2, and 3 completely abolished gC binding, suggesting minimal interaction with CS presented on the cell surface (Figure 2F). This was supported by minimal changes in cell staining after chondroitinase ABC treatment. As expected, no binding was detected on *B4GALT7* KO cells (Figure 2F). To test binding to a variety of GAG chain lengths beyond complete truncation, we additionally used a small library of glycoengineered CHO cells delineating GAG biosynthesis pathways to quantify gC binding by flow cytometry (Figure 2G) [30]. This included selective elimination of HS or CS (*EXTL2* + *EXTL3* KO and *CSGALNACT1* KO + *CSGALNACT2* KO + *CHSY1* KO, respectively), reduction in chain polymerization of HS or CS (*EXT1* KO + *EXT2* KO and *CHPF* KO, respectively), elimination of HS N-sulfation, also effectively diminishing follow-up O-sulfation (*NDST1* KO + *NDST2* KO), as well as elimination of 4-O sulfation of CS and dermatan sulfate (DS) units of CS chains (*CHST11* KO + *CHST12* KO + *CHST13* KO + *CHST14* KO). In addition, we used *B4GALT7* KO and *B3GAT3* KO cells to truncate all GAGs to initiating xylose and a short linker trisaccharide, respectively (Figure 2G). In agreement with HaCaT cell staining data, manipulation of HS synthesis and chain length substantially decreased gC binding, which was entirely dependent on HS sulfation (Figure 2H). Manipulating CS synthesis only slightly decreased gC binding, which was not dependent on the

predominant 4-O sulfation (Figure 2H). As expected, truncation to linker also completely eliminated gC binding (Figure 2H). To our surprise, some binding was retained upon complete GAG truncation, which may represent unspecific binding due to gross changes in the glycocalyx. In conclusion, by using cell surface presented GAGs, we were able to identify sulfated HS as the major contributor to HSV-1 gC binding and show that CS sulfation is not necessary for interaction with CS.

Viral assembly and properties of progeny virus

To further dissect the importance of glycans at the different stages of HSV-1 infectious cycle, we looked at viral protein expression and properties of progeny virions.We first investigated the glycoprotein expression patterns (gD and gB) in cells with the most pronounced effect on propagation using a GFP-labelled HSV-1 allowing us to also visualize the viral capsids.

In WT and *ST3GAL1* KO cells, most of gD signal was confined to the cell surface, partially overlapping with E-cadherin (Figure 3A). *ST3GAL1* KO cells exhibited much stronger gD signal, which could help explain accelerated virion production. In contrast, *C1GALT1C1* KO, *C1GALT1* KO and *MGAT1* KO cells exhibited a more disperse gD immunostaining pattern including cytoplasmic accumulation and an overall weaker signal, suggesting issues with envelope glycoprotein trafficking (Figure 3A). Compared to gD, HSV-1 gB primarily localized to the perinuclear compartment and secondary envelopment sites, as well as some surface presentation, consistent with the literature (Figure 3B) [31]. gB in *C1GALT1C1* KO, *C1GALT1* KO and *MGAT1* KO cells exhibited poorer surface and perinuclear localization compared to WT and *ST3GAL1* KO cells and presented in large clusters within the cell (Figure 3B). This could suggest defects in viral particle formation due to suboptimal viral protein incorporation in cells lacking N- and O-linked glycan maturation, which would fit with the observed diminished titers or loss of fitness.

While inspecting envelope glycoprotein localization, we also observed some differences in the localization of viral capsids. The viral capsids were found in nuclear assembly compartments, outer nuclear rim, as well as transitioning through the cytosol in WT and *ST3GAL1* KO cells. In *C1GALT1C1* KO cells, lower numbers of capsid assembly sites were seen in the nucleus, rarely

associating with the outer nuclear membrane. This was partially but to a lower extent reflected in *C1GALT1* KO and *MGAT1* KO cells (Figure 3A, 3B).

We further explored the viral replication dynamics in WT and *C1GALT1C1* KO cells by live imaging of the GFP-labelled HSV-1. Features seen in thin optical sections (Figure 3A, 3B) were also reflected in widefield images (Figure 3C). In WT cells at 14 hpi, multiple capsid assembly sites could be seen in the nucleus and capsids were also associating with the nuclear envelope in most cells irrespective of the viral load (Figure 3C). In *C1GALT1C1* KO cells less and smaller assembly sites could be seen, capsids less frequently associating with nuclear envelope, which slightly improved later in infection (20 hpi) (Figure 3C).

In order to evaluate the contribution of viral glycans to fitness of progeny virus to early interactions with wild type host cells, we took equal numbers of infectious particles produced in propagation experiments, and added to wild type keratinocyte monolayers following the previously outlined strategy. Results have revealed, that viral particles that are infectious exhibit no defects in binding or entry (Figure 3D-H). In fact, virions lacking O-glycan elongation are capable of accelerated binding, despite low viral titers of HSV-1 produced in *C1GALT1C1* KO or *C1GALT1* KO (Figure 3F). This suggests the observed propagation defects are related to formation of infectious virions rather than properties of all virions with immature O-glycans.

Role of site-specific O-glycosylation

It has been suggested that eliminating site-specific O-glycosylation can have a more profound effect on protein function than truncation of the O-glycan structure [5, 32, 33]. Therefore, although O-glycan truncation had no effect on properties of infectious virions, it should not be excluded that individual O-glycosylation sites could play a role in viral function. We have previously identified more than 70 O-glycosites on eight out of the 12 HSV-1 surface proteins, including the indispensable fusion machinery comprised of gB, gD, gH, and gL. Based on available high resolution structural data and defined molecular mechanisms, we selected a number of promising O-glycosites on gB and gD that are the most likely to affect fusion and receptor binding, respectively. We chose five out of 21 gB O-glycosites and three out of five gD O-glycosites (Figure 4A, 4F) [15]. We then generated Ser/Thr to Ala substitutions alone or in combination to test cell-

cell fusion efficiency using a split luciferase reporter assay (Table S2, Figure S1). The assay quantifies fusion between two cell types, one (effector) lacking HSV-1 entry receptors and transfected with plasmids encoding the conserved fusion machinery, and the other (target) presenting HSV-1 entry receptors (Figure 4B) [34]. Each cell type is also transfected with plasmids encoding half of a split luciferase reporter, which upon cell fusion can form a functional enzyme generating luminescence upon addition of a substrate. In addition, we quantified gB and gD surface expression by CELISA (Figure 4B) [34].

For gB single site mutants, we focused on the domain directly involved in fusion (I), where we identified three sites on antiparallel beta strands (T169, T267, T268), as well as the arm domain (V) comprised of two alpha helices that undergo structural rearrangements upon fusion, where we found one O-glycosite on each (T690 and T703) (Figure 1A) [15, 35, 36]. All mutations except for T268A affected gB cell surface expression, where T169A, T267A, and T703A had a moderate reduction in surface presentation, whereas T690A increased gB surface expression (Figure 4C). T268A exhibited reduced fusion activity despite normal expression levels, and so did T267A, even after accounting for reduced surface expression. Double or triple mutations in domain I severely decreased surface presentation also reflected in protein activity (Figure 4D). Interestingly, T690A exhibited very low fusion activity despite increased surface expression, whereas T703A was hyperfusogenic once adjusted for cell surface content. The domain V double mutant (T690A T703A) had a higher surface expression, and the fusion activity was a sum of the opposite effects of individual mutations, yielding lower activity than the WT protein (Figure 4E).

Though gD does not directly execute fusion, it initiates entry by binding to several different host cell surface receptors and reduced or impaired binding would translate to reduced fusion efficiency. For gD we selected one site on the N-terminal tail of the protein (S33 (8)), involved in interaction with both Nectin-1 and HVEM, as well as two sites on an alpha helix undergoing structural changes upon interaction with HVEM (T255 (230) and S260 (235)) (Figure 4F) [15, 37-39]. All single and compound mutants maintained close to normal levels of cell surface expression and fusion activity, which translated to slightly higher activity after surface expression adjustment (Figure 4G, 4H). Since HEK293 cells express several different receptors for gD, it is likely that alternative receptor usage would rescue inefficient binding to one of the receptors. It would

therefore be useful to explore cell lines expressing one entry receptor at a time to evaluate the effects of O-glycosite mutations on isolated interactions.

Spread of HSV-1 in mutant cell lines

Lastly, we aimed to investigate the role of glycans in cell-to-cell spread. We both measured the diameters of lesions in standard plaque assays and also looked at HSV-1 spread in 3D skin cultures and visualized the tissue lesions by immunofluorescence (Figure 5A). On wild type cell monolayers, the median plaque size was approximately 1000 microns (Figure 5B). Markedly reduced cell-to-cell spread was observed in cells devoid in N-linked glycan maturation (*MGAT1* KO) and those lacking MGAT4B (*MGAT4B* KO; *MGAT5+MGAT4B* KO) resulting in reduced β4-antenna branching (Figure 5B). Surprisingly, accelerated spread was observed in *MGAT4A* KO cells, which also contributes to β4-antenna branching, and a similar tendency was observed for *MGAT5* KO, devoid in β6-linked antenna branching. In addition, perturbations in the core 1 O-glycan biosynthetic pathway also resulted in increased plaque size, most notably in *C1GALT1* KO and *ST3GAL1* KO cells (Figure 5B). Upon plaque immunostainings, WT cells and knockout cells exhibiting increased plaque size showed strong gE expression on the cell surface (Figure 5C). In contrast, *MGAT1* KO cells showed less pronounced and more punctate gE expression, which may help explain the very limited spread capacity and may be directly linked to N-glycosylation sites on gE.

To assess how the virus spreads in tissue, we infected fully developed 3D epidermises built with the glycoengineered cell library (Figure 5D). Strikingly, very different spread characteristics were observed, when viral spread was not limited to cell-to-cell contacts mediated by gE/gI complex, but virion-to-cell spread was also permitted. In wild type skin equivalents, uniform restricted trans epidermal lesions were observed at 36 hpi (Figure 5E, 5F). To avoid selection bias, we generated ten subsequent tissue sections separated by 30 microns and scanned whole sections to visualize HSV-1 lesions, which allowed to follow lesion development throughout the tissue (Figure 5D, 5E). We identified lesions spanning several sections and measured the cross-section areas corresponding to the central regions of those lesions (Figure 5G). Extensive large lesions were seen in *MGAT1* KO tissues, in contrast to very small plaques observed in 2D (Figure 5F, 5G). In contrast, most N-glycan branching knock out tissues, most notably *MGAT4A* KO and *MGAT5+4B*

KO, permitted only limited spread in the top layers of the epidermis. *MGAT4B* KO tissue allowed formation of slightly bigger lesions, but the tissue penetrance was limited, which was also the case for tissues with reduced core 1 sialylation (*ST3GAL1* KO) (Figure 5F, 5G). No significant spread defects were noted for tissues with disruptions in GSL and GAG synthesis.

Discussion

We utilized a genetically engineered keratinocyte library to globally and systematically investigate the contributions of different classes of glycan structures to multiple stages of HSV-1 life cycle in the natural context of infection. With this strategy we discovered that each class of glycans modulated select stages of the viral life cycle, and by our approach we narrowed down the critical biosynthetic steps mediating these effects. We found chain-specific GAG sulfation, GSL sialylation and antenna-specific N-glycan branching important for attachment, O-glycan core synthesis important for propagation, and complex N-glycans important for cell-to-cell and tissue spread. In addition, reducing the complexity of the O-glycome potentiated virus-to-cell attachment, and cell-to-cell spread. Since distinct glycan classes could independently finetune early virus-host interactions, we suggest that HSV-1 through its evolution developed elaborated mechanisms to exploit the host glycosylation machinery.

Investigating the importance of complex N-linked glycans, we saw significantly smaller plaque size in *MGAT1* KO cells, indicating diminished cell-to-cell spread, while viral titers were only marginally reduced. Both observations are in accordance with previous investigations in a ricin-resistant baby hamster kidney cell line RicR14, deficient in MGAT1 activity, where similar titers were obtained in WT BHK and RicR14 cell lines deficient in complex N-linked glycans [40]. In contrast to the previous studies, we did, however, observe an increase in the ratio of total to infectious particles, and an altered localization of envelope glycoproteins gB and gD, suggestive of less productive assembly in cells lacking complex N-glycans. Furthermore, we detected lower adsorbtion of HSV-1 to *MGAT1* KO cells. In another ricin resistant cell line, Ric21, presenting with N-linked glycans of reduced complexity and sialylation HSV-1 infection also showed smaller plaque size and retarded particle production [41], suggesting the effects we see in *MGAT1* KO cells may be related to lack of sialylation. Accordingly, treatment of HSV-1 viral particles with α2,6 specific neuraminidase has

previously been shown to dramatically reduce the infectivity of viral particles [42]. However, we did not observe diminished binding of infectious particles bearing immature N-glycans lacking sialylation despite N-linked glycans being the major acceptors of α2,6-linked sialic acids in keratinocytes.

The use of cell lines defective in N-glycan branching allowed us to differentiate between contribution of β4-linked and β6-linked antennae and compare it to complete loss of N-glycan maturation. While we did not see any importance of β6-linked antennae, generated by MGAT5, we found decreased binding of wild type HSV-1 to and diminished cell-to-cell spread in *MGAT4B* KO cells, which is the main contributor to β4-linked antenna synthesis. Interestingly, MGAT4A, another isoform capable of generating β4-linked antennae, selectively reduced entry to host cells and dramatically increased HSV-1 spread in mutant cell monolayers. Since MGAT4A only has minor contribution to total cellular N-glycoprofile, this suggests the importance of protein-selective and site-specific effects. MGAT4A and MGAT4B are differentially expressed with MGAT4B being most ubiquitously expressed [43] and differential substrate protein preferences have recently been shown *in vitro* possibly regulated via the C-terminal lectin domain [27, 44]. The distinct effects of the two enzymes are also demonstrated in *MGAT4A* KO mice presenting with hyperglycemia due to selective N-glycan branching of the GLUT2 transporter by MGAT4A, despite the co-expression of MGAT4B in the pancreas [43, 45]. In contrast, it seems that MGAT4A to a large extent can compensate for MGAT4B in deficient mice due to transcriptional regulation, where no such regulation is reported for MGAT4B [43, 46]. Moreover, glycosyltransferases have been described to form complexes with each other and with nucleotide sugar transporters in the Golgi membrane, and it has been shown that MGAT1 interacts with MGAT4B, but not MGAT5 [47]. It is therefore possible, that such complex formation or lack thereof is affecting secretory pathway dynamics and protein substrate selectivity. This may help explain the comparable effects on virus-cell binding and cell-cell spread for *MGAT1* KO and *MGAT4B* KO suggesting importance of select N-glycosylation by MGAT4B of specific cellular proteins. Altogether this could help explain why we see distinct effects of MGAT4A on viral functions, although the actual mechanism is still elusive.

We previously demonstrated the importance of mucin type O-glycan elongation for HSV-1 propagation and early immune sensing [15, 48]. Here, we dissected the O-glycan biosynthetic pathway to include branching and capping steps. We discovered that the decreased viral titers and

fitness were associated with complete truncation of O-glycans to α-GalNAc by knock out of *C1GALT1* or its chaperone *C1GALT1C1*, and not with loss of sialylation of core 1 structures by ST3GAL1 or core 2 branching by GCNT1. In fact, lack of core 2 structures on host cells resulted in accelerated binding and thus entry of WT virus to cells. This is not surprising, given that core 2 structures comprise a significant portion of the cellular O-glycome, and loss of such structures reduces the complexity of structures found on the cell surface, which in turn would allow better accessibility to HSV-1. Loss of O-glycan elongation affected envelope glycoprotein localization, with lower gD surface presentation, as well as altered gB localization, which may influence their incorporation into viral particles and in turn affecting the proportion of particles capable to undergo a productive infection. In addition, gB is needed for de-envelopment at the outer nuclear membrane [49], and perturbed localization due to loss of O-glycans could contribute to lower rate of release of capsids to the cytosol. In contrast, loss of core 1 elongation or sialylation allowed for accelerated cell-to-cell spread mediated by HSV-1 gE and gI, where competent surface expression of the former protein suggests protein-selective effects of O-glycans for proper localization.

We have previously shown that HSV-1 and other herpesviruses are heavily O-glycosylated, with most surface proteins decorated with O-glycans [15, 50]. It thus may be necessary to investigate their functions in isolation to truly appreciate the structure- and site-specific roles of O-glycosylation. In an attempt to distinguish the roles of global changes of O-glycan structures on all viral proteins from the impact of losing specific O-glycosites we focused on an isolated assay probing viral protein-induced membrane fusion upon elimination of specific O-glycan acceptor amino acids on gB and gD. On fusion effector gB, we selected three O-glycosites (T169, T267, T268) decorating the central region of the antiparallel beta sheet terminating in fusion loops at the apex of domain I, and two O-glycosites (T690, T703) present on the internal alpha helices reinforcing trimer interactions and undergoing extensive reorientation upon fusion (domain V) [15, 35, 36]. While we did not expect for the specific glycans to directly be involved in membrane fusion, we hypothesized that their critical positioning may modulate the conformational stability of respective domains and their rearrangements. We saw a clear effect on cell surface expression and function of gB when eliminating specific O-glycan acceptor sites within domains directly or indirectly involved in fusion (I and V, respectively), where some mutations diminished fusion (T267A, T268A, T690A) and others accelerated it (T703A). One of the positions (T690) has

independently been identified to reduce gB function by linker insertion mutagenesis, where reduced cell surface expression was also seen [51], which is in contrast to our observed increased surface presentation of T690A mutant. None of the mutations have previously been identified by serial passage of HSV-1, and hyperfusogenic mutations in gB ectodomain are rare, which are normally found in the cytoplasmic tail [52, 53]. Such mutations have been shown to affect the stability of the trimer in the pre-fusion conformation and the energy barrier threshold for executing fusion [54]. It will be important to validate the effect is truly glycan dependent and not influenced by the change in amino acid itself, and also to define O-glycan occupancy on HSV-1 virions. Nevertheless, the work identifies new hotspots in gB structure that could be targeted for disrupting protein function. In contrast, infectious virions bearing truncated O-glycans did not exhibit any defects in binding or entry; in fact, we observed accelerated binding, suggesting that even very short O-glycans are sufficient for maintaining functions of properly localized proteins.

In addition to investigating roles of protein glycosylation in herpesvirus biology, we also addressed the functions of two other major classes of cell-surface glycoconjugates: GAG-bearing proteoglycans and GSLs. It is noteworthy mentioning that most of the studies investigating the roles of GAGs and GSLs are based on isolated systems involving synthetic (glyco)conjugates and isolated or overexpressed viral proteins, often in non-permissive cells. While such studies are instrumental for defining and quantifying molecular interactions, and sophisticated approaches are taken to mimic cell surface composition and curvature, they provide limited biological context. In contrast, we explored the role of cell-surface presented and native core-protein bound structures, demonstrating that binding of viral particles to cell monolayers bearing GAG-devoid proteoglycans on ice was almost completely inhibited, emphasizing the role of GAGs in very early interactions. Surprisingly, the effect was less pronounced if adsorbtion was allowed at 37 °C with occasional agitation (data not shown), and HSV-1 propagated well in *B4GALT7* KO cells. This underscores the contextualized functions of glycans as modulators of molecular interactions, which only become obligate under specific stress conditions [6]. Our findings are in agreement with the well documented role of glycosaminoglycans in herpesvirus biology [24, 25, 55-57]. It is proposed that GAGs allow HSV particles to “surf” on the cell surface until encountering cognate receptors for gD and initiating entry. Lack of such interactions has been demonstrated to prevent

free movement of the viral particles on membrane equivalents or the surface of cells [56, 58]. While HSV-1 can interact with both HS and CS in solution or on solid support [25, 28, 29], little is known regarding the interaction with GAGs attached to their intrinsic core proteins on intact cells in the context of the remaining glycocalyx. We determined that N-sulfated HS is the major contributor of HSV-1 gC binding to CHO cells, with a minor contribution from CS, not dependant on sulfation. By selective desulfation of purified HS, it has previously been shown that 2-O, 6-O, and N-sulfation, and at least a fragment of 12 monosaccharides is needed for optimal gC-HS interaction [29]. gC was still able to bind de-N-sulfated HS partially [29], suggesting that N-sulfation, genetic depletion of which completely abolished gC binding in our study, is also important for creation of sulfate-rich GAG patches by follow-up 2-O and 6-O sulfation.

After attachment, HSV-1 enters keratinocytes either via direct membrane fusion or endocytosis, and both of these routes are thought to be cholesterol-rich lipid raft dependant and involving interactions between viral and cellular proteins [23, 26, 59-61]. Mechanistic insight into the interaction of sphingomyelin and cholesterol with HSV-1 gH leading to membrane fusion is available [62]. In contrast, knowledge on the role of glycosphingolipids, another major component of lipid rafts, in HSV-1 biology is scarce. Here, we show that elongation of host GSLs beyond glucosylceramide is important for efficient viral binding and entry. It is suggested that αVβ3-integrin reroutes nectin 1 to lipid rafts thus promoting cholesterol-mediated entry [63]. It is therefore plausible that altering the composition of lipid rafts by changing the GSL content may interfere with proper nectin 1 trafficking as well as membrane fusion dynamics via gH.

In further attempts to examine contextualized functions of glycans in a biologically relevant system, we utilized the ability of keratinocytes to form stratified epithelia to investigate viral spread in glycoengineered tissue. Strikingly, we saw very different effects of glycans in 3D tissue spread compared to overlaid monolayers. This suggests the effects we see in 2D are directly related to importance of glycans on gE/gI complex or their receptors, whereas 3D spread involves both cell-to-cell and virus-to-cell transmission, and is also influenced by changes in tissue architecture induced by glycogene knock outs.

In addition to uncovering various functions of distinct classes and subtypes of cellular glycans, we also shed light on the requirement of viral glycans for proper function. HSV-1 particles are shown to contain both N-linked and O-linked glycans, and it is expected glycosphingolipids are part of the

cell membrane-derived viral envelope [15-18]. It is not known whether proteoglycans decorated with GAGs can be incorporated into HSV-1 particles, but they were not detected in a proteomic study looking at cellular proteins incorporated into HSV-1 membranes [64]. While we identified ample functions of cellular glycans in HSV-1 biology, we found limited effects of glycome perturbations on properties of progeny virions able to establish infection, apart from accelerated binding of virions bearing truncated O-glycans. This further supports that missing elongated O-glycans limits the assembly of infection-competent virions in the host cell rather than limiting the successive infection.

By using a glycoengineered keratinocyte library, we show that different classes and even subtypes of glycans play very selective and mostly dispensable roles in specific stages in HSV-1 life cycle, importance of which only becomes evident under suboptimal conditions. We conclude that HSV-1 developed an elaborate network of interactions with different cellular glycans allowing for efficient entry and propagation, which could be explored for glycan-targeted intervention strategies. Individual findings of this exploratory study shall be the scope of future investigations.

Materials and methods

Cells and viruses

The HaCaT human keratinocyte WT and genetically engineered cell lines were grown in DMEM supplemented with 10 % FBS (HyClone) and 4 mM L-glutamine. CHOZN GS -/- (glutamine synthetase KO; WT CHO (Sigma)) and genetically engineered cell lines [30] were grown in EX-CELL® CD CHO Fusion serum free media mixed 1:1 with BalanCD CHO growth media and supplemented with 2 % L-glutamine in 50 mL TPP TubeSpin® Bioreactors. DMEM mixed 1:1 with Ham's F12 nutrient mix and supplemented with 10 % FBS (Gibco) and 4 mM L-glutamine was used for adherent CHO cell culture. HEK293 Ac2 cells were grown in DMEM supplemented with 10 % FBS (Gibco) and 4 mM L-glutamine. The wild-type HSV-1 virus Syn17+ [65] was used throughout the study, and the virus titers were determined by plaque titration on Green monkey kidney (GMK, obtained from the Swedish Institute for Infectious Disease Control, Stockholm) cells as previously described [66]. HSV-1 Syn17+ virus was cultivated in HaCaT wild type keratinocytes or GMK cells depending on downstream application and the titers were determined as mentioned above.

K26GFP HSV-1 [67] was a kind gift from Prashant Desai (The Johns Hopkins University), and cultivated as mentioned above.

ZFN and CRISPR/Cas9 gene targeting

HaCaT KO library was generated using ZFN nuclease and CRISPR/Cas9 technology by targeting particular glycogene exons by validated gRNAs [68] or gRNAs predicted by GPP [69]. gRNAs were cloned [70] using oligos (TAGC, Denmark) into lentiCRISPR-v2-Puro plasmid backbone (Addgene #52961) or lentiCRISPR-v2-Blast with a blasticidin resistance gene replacing the puromycin resistance gene (Brakebusch laboratory, BRIC, UCPH, DK). Directional cloning and insertion of the gRNA duplex using BsmBI and T4 ligase into the LentiCRISPR-v2 plasmid backbone was done as described earlier [71]. All plasmids were propagated in One Shot™ Stbl3™ Chemically Competent *E. coli* cells (Thermo Fisher). Endonuclease free plasmid preparations were made using Midi Prep kit (Thermo Fisher). For lentivirus production HEK293T cells were seeded at $1x10^5$ cells/well density in a 6-well plate and grown for 72 h until 80-90% confluence. For transfection, 200 µL OPTI-MEM (Gibco), 8 µL of 1 mg/mL PEI (Sigma), 0.8 µg LentiCRISPR-V2-gRNA plasmid, 0.6 µg pCMV-VSV-G plasmid (Addgene #8454), and 0.6 µg psPAX2 plasmid (Addgene #12260) were mixed and incubated for 10 min at RT before added to the adherent HEK293T cells. After 24 h the transfection media was replaced with HaCaT media for harvesting virus for transduction. Medium containing viral particles was collected 48/72 h post-transfection, i.e. when virus had accumulated for 24 h after medium change, filtered (0.45 µm pore size). Filtered virus-containing medium was mixed 1:1 with fresh HaCaT media and 1:1000 polybrene (Sigma), and used to transduce HaCaT cells overnight [72]. Selection of KO cell lines started 48-96 hours after transduction, with either 5 µg/ml blasticidin S (Gibco) or 1 µg/ml puromycin (Gibco) including biweekly cell passaging. Single clones were obtained by serial dilution in 96 well plates and KO clones were identified by IDAA using ABI PRISM™ 3010 Genetic Analyzer (Thermo Fisher) and Sanger sequencing (GATC, Germany). Two to five clones were selected for each gene with out of frame indel formation. IDAA results were analyzed using Peak Scanner Software V1.0 (Thermo Fisher) [73].

MS-based glycan profiles

For O-GalNAc profiles, the Cellular O-Glycome Reporter/Amplification (CORA) method was used as described in [74]. In brief, HaCaT cells were seeded in 6-well plates, and when the cells reached 70

% confluence, the medium was supplemented with 100 µM Bn-α-GalNAc or DMSO for untreated controls. Media was harvested after 48 h and passed through a 10-kDa Omega membrane (Pall Corporation) followed by purification with a Sep-Pak 3-cc C18 cartridge (Waters). Samples were then concentrated by SpeedVac to remove organic solvent and lyophilized. For profiling of N-linked glycans, HaCaT cell pellets were dissolved in 0.1 % Rapigest (Waters) and incubated on ice and vortexed every 5 minutes. Samples were then centrifuged at 10000 g for 10 min and the supernatant was collected and reduced with 5 mM DTT (Sigma) for 1 h at 60 °C followed by alkylation with iodoacetamide (Sigma) for 30 minutes at RT while kept dark. Samples were digested with 5 µg trypsin (Roche Diagnostics) overnight at 37 °C and peptides were purified with a Sep-Pak 1-cc C18 cartridge (Waters). Organic solvent was removed by SpeedVac and pH was adjusted to 7-8 with 50 mM ammonium bicarbonate, followed by overnight digestion with 3 U PNGase F (Roche diagnostics) at 37 °C. Released N-glycans were cleaned up on a Sep-Pak 1-cc C18 cartridge and lyophilized. For N-glycan profiles, dried samples were permethylated as described previously [75] and analysed by positive reflector mode MALDI-TOF (AutoFlex Speed, Bruker Daltonics) with data acquisition in the 1000-5000 m/z range. For O-glycans the data acquisition was in the 500-3500 m/z range.

Organotypic culture

Organotypic cultures were prepared as described by Dabelsteen et al. [33, 76]. Briefly, human fibroblasts were suspended in acid-extracted type I collagen (4 mg/mL) and allowed to gel over a 1-mL layer of acellular collagen in six-well culture inserts with 3-µm-pore polycarbonate filters (BD Biosciences NJ, USA). Gels were allowed to contract for 4–5 days before seeding with $3x10^5$ HaCaT keratinocytes in serum and mitogen-supplemented DMEM/F12 raft medium. Inserts were raised to the air-liquid interface 4 days after cell seeding, and the media changed every second day for an additional 10 days. Infection of organotypic cultures was performed as previously described with minor modifications [77]. Briefly, media was removed on day 9 after insert raising, and 3000 PFU of HSV-1 Syn 17+ applied in 500 µL of RAFT media to the to the top of the cultures, let drip through in 15 min, and reapplied 3 more times during 1 hour. RAFT media was then added to cover the bottom of the organotypic cultures and incubated for 36 more hours until harvesting.

Propagation assay

HaCaT cell monolayers in 6 wells in triplicates were washed with PBS and infected with MOI 10 of HSV-1 Syn 17+. The virions in 1 mL of DMEM P/S were adsorbed at 37 °C with periodical rocking of the plates for 1 hour, inoculum removed and cells washed with PBS, followed by addition of 2 mL/well of DMEM supplemented with 10 % FCS and P/S. Virus was harvested at 17 hours post infection. Media was spun at 3000 rpm for 10 min at 4 °C, supernatant aliquoted and stored at -80 °C. Cell monolayers were washed with PBS, dissociated with TrypLE reagent, spun at 100 x g for 5 min, washed with PBS, aliquoted and spun at 400 x g for 5 min, supernatant removed and cells stored at -80 °C.

Plaque assay

Titers of virus produced in HaCaT keratinocytes were determined on Green monkey kidney (GMK) cells. Cell monolayers were infected with serial dilutions of virus and allowed to attach. After 1 h the inoculum was removed and the cells overlaid with medium containing 1 % methylcellulose (Sigma-Aldrich), 2.5% FCS, 100 unit/mL penicillin and 100 µg/mL streptomycin (in HBSS (Sigma-Aldrich) + DMEM (Gibco, Life Technologies) at a ratio of 1:1). After 48 h incubation, the overlay medium was removed, the cells fixed with 1 % crystal violet (in 70 % EtOH/37 % formaldehyde/acetic acid 20:2:1 v/v/v), washed 4x times with water and allowed to dry. The resulting plaques were inspected and counted using a light microscope (Olympus IMT-2). Plaque size was measured using AxioVision software.

DNA extraction and qPCR

DNA was extracted using the NucleoSpin® Tissue Kit (Macherey-Nagel) according to manufacturer's instructions. Media was diluted 200x before extraction and 100 µL used for extraction. DNA was eluted in 100 µL volume. For assessing the DNA copy number of HSV-1, a 118-nucleotide segment of the gB-1 region was amplified with primers described in [78]. The qPCR reaction volume was set to 20 µL and contained 4 µL HOT FIREPol®Probe qPCR Mix Plus (ROX) (Solis Biodyne), primers and probe (forward primer at 0.5 µM, reverse primer at 0.5 µM and probe at 0.3 µM final concentrations), and 1 µl of DNA. Amplification of the target sequence was performed using the StepOne Plus system (Thermo Scientific). The reaction conditions were set to 10 min at 95 °C followed by 45 PCR cycles of two-step amplification (15 sec at 95 °C and 60 sec at 60 °C). HSV-1 Forward 5'-GCAGTTTACGTACAACCACATACAGC-3'; HSV-1 Reverse 5'-AGCTTGCGGGCCTCGTT-3';

HSV-1 Probe FAM-5'-CGGCCCAACATATCGTTGACATGGC-3'-MGBNFQ (Thermo Fisher Scientific). The efficiency of each round of PCR was determined using 10-fold dilutions of Topo TA plasmids (Invitrogen AB, Stockholm, Sweden) with insert of respective amplicon created according to the manufacturer's instructions.

Binding and entry assays

Binding and entry assays were performed as previously described [79]. HaCaT cell monolayers were prechilled on ice for 30 min. For binding assay, 200 PFU of HSV-1 Syn 17+ WT or glycoengineered HSV-1 in 1 mL DMEM supplemented with 2.5 % FCS, 100 unit/mL penicillin and 100 µg/mL streptomycin (P/S) was added on cell monolayers on ice in triplicates, and incubated for 20 or 120 min. After the indicated time points, cells were washed twice with ice-cold PBS and overlain with 2 % methylcellulose in HBSS, mixed 1:1 (v/v) with DMEM supplemented with 5 % FCS, 200 unit/mL penicillin and 200 µg/mL streptomycin. Overlain monolayers were incubated at 37 °C and 5 % CO_2 for 48 h, overlay media removed, cells fixed and stained with 1 % crystal violet in 70 % EtOH/37 % formaldehyde/acetic acid (20:2:1 v/v/v), washed 4 times with MQ H_2O, dried, and plaques counted using a light microscope (Olympus IMT-2). For entry assay, after 120 min on ice, the inoculum was removed, washed with room temperature DMEM, P/S, and 1 mL of room temperature DMEM supplemented with 2.5 % FCS and P/S was added, followed by a 5 min incubation at 37 °C. The plates were then returned on ice, media removed and non-entered particles inactivated with ice-cold citrate buffer (40 mM citric acid, 10 mM KCl, 135 mM NaCl pH 3) for 2 min, then washed twice with ice-cold PBS and overlain with media as described above. A 0 min time point without shift to 37 °C was used as control.

Antibodies and probes

Mouse anti-gB (HSV-1B11D8), anti-gC (B1C1B4), anti-gD (C4D5G2) and anti-gE (B1E6A5) mAbs, as well as recombinant gC probe were kindly provided by Tomas Bergström and Rickard Nordén (University of Gothenburg). Rabbit anti-E-cadherin mAb (24E10) was purchased from Cell Signaling Technology and goat anti-HSV-1-FITC pAb (GTX40437) from Genetex. Goat anti-mouse IgG AF647 $F(ab)_2$, goat anti-mouse IgG AF594 (H+L), goat anti-mouse IgG AF488 (H+L), and donkey anti-rabbit IgG AF546 (H+L) were all from Thermo Fisher Scientific. Rabbit anti-mouse Igs HRP was from DAKO.

Immunofluorescence

HaCaT cells grown on glass cover slips in 24-wells were infected with MOI 10 of HSV-1 K26-GFP. 14 hours post-infection the cells were washed 2x with Hanks' Balanced Salt solution (HBSS, Sigma-Aldrich Cat. Nr. H8264) and fixed with 4 % PFA in PBS (Ampliqon Cat. Nr. AMPQ44154.1000) for 15 min at RT followed by 2x more washes. The cells were permeabilized with 0.3 % Triton X-100 in HBSS for 3 min followed by 2x washes with HBSS and blocked with 2.5 % BSA in HBSS, 0.03 % sodium azide at RT for 45 min. Cover slips were incubated with primary antibodies diluted in blocking buffer at 4 °C over night followed by 3x washes with HBSS and incubation with secondary antibodies at RT for 45 min. The cover slips were rinsed with HBSS and incubated with 0.1 µg/mL DAPI solution in HBSS for 5 min followed by 3x washes and mounting with Prolong Gold antifade-reagent (Thermo Fisher Scientific Cat. Nr. P36930). For stainings of non-infected HaCaT cells with gC probe, fixed and permeabilized cells on cover slips were treated with either chondroitinase ABC, heparinases 1, 2 and 3, or left untreated for 1 hour at 37 °C followed by incubation with 2 µg/mL gC probe diluted in 2.5 % BSA in PBS, 0.03 % sodium azide for 1 hour at RT, 3x washes with PBS and staining with mouse anti-gC mAb as described above, though using PBS-based blocking buffer and washes. For plaque stainings HaCaT cells grown on large cover slips in 6 wells were infected with 200 PFU of HSV-1 K26-GFP and overlaid with DMEM, 2.5 % FCS, 1 % methylcellulose, 100 unit/mL penicillin, 100 µg/mL streptomycin for 48 hours. Therafter the overlay media was removed, cover slips washed 3x with PBS and fixed in 4 % PFA in PBS for 25 min followed by 3x washes and blocking in 2.5 % BSA in PBS, 0.03 % sodium azide at 4 °C over night and staining procedure as described above, though with primary Ab incubation for 2 hours at RT and dilutions in 2.5 % BSA in PBS, 0.03 % sodium azide. For stainings of non-infected HaCaT cells with gC probe, fixed and permeabilized cells on cover slips were treated with either chondroitinase ABC, heparinases 1, 2 and 3, or left untreated for 1 hour at 37 °C followed by incubation with 2 µg/mL gC probe for 1 hour at RT, 3x washes with PBS and staining with mouse anti-gC mAb as described above. Images were documented using Zeiss LSM710 confocal microscope. FFPE organotypic tissue sections were deparaffinized and microwave treated for antigen retrieval (Tris-HCl buffer pH 9). The sections were then permeabilized with 0.3 % Triton X-100 in PBS, washed 3x and incubated with goat anti-HSV-1-FITC pAb (GeneTex, 1:50 in 2.5 % BSA in PBS, 0.03 % NaN_3) for 2 h at room temperature, followed by 3 washes with PBS and mounting with ProLong™ Gold antifade reagent

with DAPI (Thermo Fisher Scientific). Entire sections were imaged using Zeiss AxioScan microscope. Images were assembled using Adobe Photoshop 2021, Adobe Illustrator 2021, or Zeiss ZEN Lite software.

Flow cytometry

Cell surface binding studies were carried out by flow cytometry analysis. First, cells were counted and 1 x 10^5 cells/well were distributed into U-bottom 96-well plate (TermoFisher Scientific™ Nunclon™ Delta surface). Cell viability was evaluated by trypan blue stain, applying a viability requirement of > 95 % for cells to be included for analysis. Next, cells were washed once in ice-cold PBS, centrifuged at 500 x g for 3 min at 4 °C. Cells were then incubated with recombinant gC protein (0.5 µg/mL) diluted in ice-cold PBS with 2 % FBS, for 45 min at 4°C. Following, cells were washed twice in ice-cold PBS with 2 % FBS before incubation with mouse anti-gC mAb B1C1B4 (2 µg/mL) diluted in PBS with 2 % FBS for 45 min at 4 °C. After incubation, cells were washed twice in ice-cold PBS with 2 % FBS and incubated with goat anti-mouse IgG (H+L) AF488 (1:1000) diluted in PBS with 2 % FBS for 45 min at 4 °C in the dark. Lastly, cells were washed twice with PBS with 2 % FBS, and suspended in 100 µL PBS with 2 % FBS for analysis. Fluorescence intensity was measured on the SONY Spectral Cell Analyzer (SONY SA3800). A total minimum of 10 000 events were recorded for analysis. Cell debris and doublets were excluded based on FSC-A/FSC-H plot to ensure analysis based on singlets. Data is presented as the geometric mean of samples incubated with gC probe, after substraction of the geometric mean of background fluorescence, samples incubated with primary and secondary antibody only, and normalized to WT. All data analysis was done using FlowJo V. 10.0.7.

Plasmids and cloning

Plasmids encoding full length HSV-1 gB (pMTS-1-gB), gD (pcDNA3.1(-)-gD), gH (pMTS-1-gH), and gL pMTS-1-gL) was a kind gift from Gabriella Campadelli-Fiume (University of Bologna). Plasmids encoding split luciferase (DSP1-7, DSP8-11) were kindly provided by Zene Matsuda (University of Tokyo). Single and multiple amino acid mutations in gB and gD were introduced using custom primers (Table S2) and the QuikChange Lightning Multi Site-Directed Mutagenesis Kit according to manufacturer's instructions. Briefly, mutagenic primers were annealed and extended during 30 thermal cycles (2 min 95 °C; 30 x (20 sec 95 °C, 30 sec 55 °C, 30 sec/kb 65 °C); 10 min 65 °C),

followed by template digestion with DpnI, and transformation into XL10-Gold Ultracompetent Cells. The transformation reactions were plated on LB-carbenicillin agar plates and colonies screened by PCR using Herculase II Fusion Pfu DNA Polymerase (Agilent) followed by Sanger sequencing. Colonies of interest were re-streaked, grown up in LB-carbenicillin media and Mini Preps prepared using Zyppy Plasmid Miniprep Kit (Zymo Research) followed by Sanger sequencing. Subsequently, plasmid Midi Preps were prepared using NucleoBond Xtra Midi Endotoxin-free Kit (Macherey-Nagel).

Split-luciferase assay

The assay was performed as previously described [34] with several modifications. CHO K1 cells (effector) grown in Greiner CELLSTAR® white polystyrene 96 well plates were transfected with 375 ng/well of gB, as well as 125 ng of each gD, gH, gL, and DSP1-7 plasmids using Lipofectamine 3000 (Thermo Scientific) according to manufacturer's instructions in triplicates. Plasmids encoding wild type or mutated gB or gD were used. An additional clear polystyrene plate with transfected cells was prepared for CELISA measurements. HEK293 cells (target) grown in 6 well plates were transfected with 1 μg/well of DSP8-11 plasmid. For split-luciferase assay, 23 hours post-transfection, the media of CHO K1 cells was replaced with fusion media (DMEM (no phenol red), 5 % FCS, 50 mM HEPES), supplemented with EnduRen substrate (Promega, 1:1000) and incubated at 37 °C for 1 hour. HEK293 cells were detached using 0.02 % EDTA in PBS, resuspended in fusion media and added to effector cells. Luminescence was measured every 2 min for 240 min at 37 °C using EnSpire plate reader (Perkin-Elmer).

CELISA

Cell surface ELISA was performed as previously described [34] with several modifications. 96w plates with transfected cells were washed 3x with PBS supplemented with divalent cations (0.9 mM $CaCl_2$, 0.5 mM $MgCl_2$ (PBS^{2+})) 20 hours post-transfection and fixed with 4 % PFA in PBS for 10 min followed by 3x washes and blocking in 3 % BSA in PBS^{2+} for 30 min. The cells were then incubated with mouse anti-gB (1:20) or anti-gD (1:100) mAbs in blocking buffer for 1 hour at room temperature, followed by 5x washes and incubation with rabbit anti-mouse Igs HRP (1:500) for 45 min and 6x washes. Plates were developed using TMB + substrate chromogen (Thermo Scientific)

and stopped with 0.5 M H_2SO_4. The absorbance at 450 nm was quantified using BioTek Synergy LX plate reader.

Acknowledgements

We thank Karin Uch Hansen for technical assistance. We acknowledge the Core Facility for Integrated Microscopy, Faculty of Health and Medical Sciences, University of Copenhagen. We kindly thank Tomas Bergström, Rickard Nordén, Prashant Desai, Zene Matsuda, and Gabriella Campadelli-Fiume for sharing antibodies, plasmids, and virus strains. We also thank Rickard Nordén, Sigvard Olofsson, Tomas Bergström, Gary Cohen and Doina Atanasiu for their valuable guidance. This work was supported by Lundbeck Foundation (R219-2016-545), Danish National Research Foundation (DNRF107) and European Comission (GlycoSkin H2020-ERC).

Declaration of interests

HHW owns stocks and is a consultant for and co-founder of EbuMab, ApS, Hemab, ApS, and GO-Therapeutics, Inc. All other authors declare no conflicts of interest.

References

1. Bagdonaite I, Wandall HH (2018) Global aspects of viral glycosylation. *Glycobiology* **28**: 443-467
2. Varki A (2017) Biological roles of glycans. *Glycobiology* **27**: 3-49
3. Schjoldager KT, Narimatsu Y, Joshi HJ, Clausen H (2020) Global view of human protein glycosylation pathways and functions. *Nat Rev Mol Cell Biol* **21**: 729-749
4. Wandall HH, Nielsen MAI, King-Smith S, de Haan N, Bagdonaite I (2021) Global functions of O-glycosylation: promises and challenges in O-glycobiology. *Febs j*
5. Bagdonaite I, Pallesen EM, Ye Z, Vakhrushev SY, Marinova IN, Nielsen MI, Kramer SH, Pedersen SF, Joshi HJ, Bennett EP*, et al.* (2020) O-glycan initiation directs distinct biological pathways and controls epithelial differentiation. *EMBO Rep* **21**: e48885
6. Dabelsteen S, Pallesen EMH, Marinova IN, Nielsen MI, Adamopoulou M, Rømer TB, Levann A, Andersen MM, Ye Z, Thein D*, et al.* (2020) Essential Functions of Glycans in Human Epithelia Dissected by a CRISPR-Cas9-Engineered Human Organotypic Skin Model. *Dev Cell*
7. Büll C, Nason R, Sun L, Van Coillie J, Madriz Sørensen D, Moons SJ, Yang Z, Arbitman S, Fernandes SM, Furukawa S*, et al.* (2021) Probing the binding specificities of human Siglecs by cell-based glycan arrays. *Proc Natl Acad Sci U S A* **118**

8. Narimatsu Y, Joshi HJ, Nason R, Van Coillie J, Karlsson R, Sun L, Ye Z, Chen YH, Schjoldager KT, Steentoft C*, et al.* (2019) An Atlas of Human Glycosylation Pathways Enables Display of the Human Glycome by Gene Engineered Cells. *Mol Cell* **75**: 394-407.e5
9. James C, Harfouche M, Welton NJ, Turner KM, Abu-Raddad LJ, Gottlieb SL, Looker KJ (2020) Herpes simplex virus: global infection prevalence and incidence estimates, 2016. *Bull World Health Organ* **98**: 315-329
10. Itzhaki RF (2021) Overwhelming Evidence for a Major Role for Herpes Simplex Virus Type 1 (HSV1) in Alzheimer's Disease (AD); Underwhelming Evidence against. *Vaccines* **9**
11. Bradshaw MJ, Venkatesan A (2016) Herpes Simplex Virus-1 Encephalitis in Adults: Pathophysiology, Diagnosis, and Management. *Neurotherapeutics* **13**: 493-508
12. Tan IL, McArthur JC, Venkatesan A, Nath A (2012) Atypical manifestations and poor outcome of herpes simplex encephalitis in the immunocompromised. *Neurology* **79**: 2125-32
13. Eisenberg RJ, Atanasiu D, Cairns TM, Gallagher JR, Krummenacher C, Cohen GH (2012) Herpes virus fusion and entry: a story with many characters. *Viruses* **4**: 800-32
14. Johnson DC, Baines JD (2011) Herpesviruses remodel host membranes for virus egress. *Nat Rev Microbiol* **9**: 382-94
15. Bagdonaite I, Norden R, Joshi HJ, Dabelsteen S, Nystrom K, Vakhrushev SY, Olofsson S, Wandall HH (2015) A strategy for O-glycoproteomics of enveloped viruses--the O-glycoproteome of herpes simplex virus type 1. *PLoS pathogens* **11**: e1004784
16. Wenske EA, Bratton MW, Courtney RJ (1982) Endo-beta-N-acetylglucosaminidase H sensitivity of precursors to herpes simplex virus type 1 glycoproteins gB and gC. *Journal of virology* **44**: 241-8
17. Serafini-Cessi F, Dall'Olio F, Pereira L, Campadelli-Fiume G (1984) Processing of N-linked oligosaccharides from precursor- to mature-form herpes simplex virus type 1 glycoprotein gC. *Journal of virology* **51**: 838-44
18. Norden R, Halim A, Nystrom K, Bennett EP, Mandel U, Olofsson S, Nilsson J, Larson G (2015) O-linked glycosylation of the mucin domain of the herpes simplex virus type 1-specific glycoprotein gC-1 is temporally regulated in a seed-and-spread manner. *The Journal of biological chemistry* **290**: 5078-91
19. Geraghty RJ, Krummenacher C, Cohen GH, Eisenberg RJ, Spear PG (1998) Entry of alphaherpesviruses mediated by poliovirus receptor-related protein 1 and poliovirus receptor. *Science* **280**: 1618-20
20. Montgomery RI, Warner MS, Lum BJ, Spear PG (1996) Herpes simplex virus-1 entry into cells mediated by a novel member of the TNF/NGF receptor family. *Cell* **87**: 427-36
21. Satoh T, Arii J, Suenaga T, Wang J, Kogure A, Uehori J, Arase N, Shiratori I, Tanaka S, Kawaguchi Y*, et al.* (2008) PILRalpha is a herpes simplex virus-1 entry coreceptor that associates with glycoprotein B. *Cell* **132**: 935-44
22. Shukla D, Liu J, Blaiklock P, Shworak NW, Bai X, Esko JD, Cohen GH, Eisenberg RJ, Rosenberg RD, Spear PG (1999) A novel role for 3-O-sulfated heparan sulfate in herpes simplex virus 1 entry. *Cell* **99**: 13-22
23. Gianni T, Salvioli S, Chesnokova LS, Hutt-Fletcher LM, Campadelli-Fiume G (2013) alphavbeta6- and alphavbeta8-integrins serve as interchangeable receptors for HSV gH/gL to promote endocytosis and activation of membrane fusion. *PLoS Pathog* **9**: e1003806
24. Shieh MT, WuDunn D, Montgomery RI, Esko JD, Spear PG (1992) Cell surface receptors for herpes simplex virus are heparan sulfate proteoglycans. *J Cell Biol* **116**: 1273-81

25. Peerboom N, Block S, Altgarde N, Wahlsten O, Moller S, Schnabelrauch M, Trybala E, Bergstrom T, Bally M (2017) Binding Kinetics and Lateral Mobility of HSV-1 on End-Grafted Sulfated Glycosaminoglycans. *Biophys J*
26. Sayers CL, Elliott G (2016) HSV1 Enters Human Keratinocytes by a Nectin-1-Dependent, Rapid Plasma Membrane Fusion Pathway that Functions at Low Temperature. *J Virol*
27. Osada N, Nagae M, Nakano M, Hirata T, Kizuka Y (2022) Examination of differential glycoprotein preferences of N-acetylglucosaminyltransferase-IV isozymes a and b. *J Biol Chem*: 102400
28. Altgarde N, Eriksson C, Peerboom N, Phan-Xuan T, Moeller S, Schnabelrauch M, Svedhem S, Trybala E, Bergstrom T, Bally M (2015) Mucin-like region of herpes simplex virus type 1 attachment protein gC modulates the virus-glycosaminoglycan interaction. *The Journal of biological chemistry*
29. Feyzi E, Trybala E, Bergström T, Lindahl U, Spillmann D (1997) Structural requirement of heparan sulfate for interaction with herpes simplex virus type 1 virions and isolated glycoprotein C. *J Biol Chem* **272**: 24850-7
30. Chen YH, Narimatsu Y, Clausen TM, Gomes C, Karlsson R, Steentoft C, Spliid CB, Gustavsson T, Salanti A, Persson A*, et al.* (2018) The GAGOme: a cell-based library of displayed glycosaminoglycans. *Nat Methods* **15**: 881-888
31. Wisner TW, Johnson DC (2004) Redistribution of cellular and herpes simplex virus proteins from the trans-golgi network to cell junctions without enveloped capsids. *J Virol* **78**: 11519-35
32. Bagdonaite I, Pallesen EMH, Nielsen MI, Bennett EP, Wandall HH (2021) Mucin-Type O-GalNAc Glycosylation in Health and Disease. *Adv Exp Med Biol* **1325**: 25-60
33. Radhakrishnan P, Dabelsteen S, Madsen FB, Francavilla C, Kopp KL, Steentoft C, Vakhrushev SY, Olsen JV, Hansen L, Bennett EP*, et al.* (2014) Immature truncated O-glycophenotype of cancer directly induces oncogenic features. *Proceedings of the National Academy of Sciences of the United States of America* **111**: E4066-75
34. Saw WT, Matsuda Z, Eisenberg RJ, Cohen GH, Atanasiu D (2015) Using a split luciferase assay (SLA) to measure the kinetics of cell-cell fusion mediated by herpes simplex virus glycoproteins. *Methods* **90**: 68-75
35. Heldwein EE, Lou H, Bender FC, Cohen GH, Eisenberg RJ, Harrison SC (2006) Crystal structure of glycoprotein B from herpes simplex virus 1. *Science* **313**: 217-20
36. Vollmer B, Pražák V, Vasishtan D, Jefferys EE, Hernandez-Duran A, Vallbracht M, Klupp BG, Mettenleiter TC, Backovic M, Rey FA*, et al.* (2020) The prefusion structure of herpes simplex virus glycoprotein B. *Sci Adv* **6**
37. Carfí A, Willis SH, Whitbeck JC, Krummenacher C, Cohen GH, Eisenberg RJ, Wiley DC (2001) Herpes simplex virus glycoprotein D bound to the human receptor HveA. *Mol Cell* **8**: 169-79
38. Di Giovine P, Settembre EC, Bhargava AK, Luftig MA, Lou H, Cohen GH, Eisenberg RJ, Krummenacher C, Carfi A (2011) Structure of herpes simplex virus glycoprotein D bound to the human receptor nectin-1. *PLoS Pathog* **7**: e1002277
39. Krummenacher C, Supekar VM, Whitbeck JC, Lazear E, Connolly SA, Eisenberg RJ, Cohen GH, Wiley DC, Carfí A (2005) Structure of unliganded HSV gD reveals a mechanism for receptor-mediated activation of virus entry. *Embo j* **24**: 4144-53
40. Campadelli-Fiume G, Poletti L, Dall'Olio F, Serafini-Cessi F (1982) Infectivity and glycoprotein processing of herpes simplex virus type 1 grown in a ricin-resistant cell line deficient in N-acetylglucosaminyl transferase I. *Journal of virology* **43**: 1061-71

41. Serafini-Cessi F, Dall'Olio F, Scannavini M, Campadelli-Fiume G (1983) Processing of herpes simplex virus-1 glycans in cells defective in glycosyl transferases of the Golgi system: relationship to cell fusion and virion egress. *Virology* **131**: 59-70
42. Teuton JR, Brandt CR (2007) Sialic acid on herpes simplex virus type 1 envelope glycoproteins is required for efficient infection of cells. *Journal of virology* **81**: 3731-9
43. Takamatsu S, Antonopoulos A, Ohtsubo K, Ditto D, Chiba Y, Le DT, Morris HR, Haslam SM, Dell A, Marth JD*, et al.* (2010) Physiological and glycomic characterization of N-acetylglucosaminyltransferase-IVa and -IVb double deficient mice. *Glycobiology* **20**: 485-97
44. Nagae M, Hirata T, Tateno H, Mishra SK, Manabe N, Osada N, Tokoro Y, Yamaguchi Y, Doerksen RJ, Shimizu T*, et al.* (2022) Discovery of a lectin domain that regulates enzyme activity in mouse N-acetylglucosaminyltransferase-IVa (MGAT4A). *Commun Biol* **5**: 695
45. Ohtsubo K, Takamatsu S, Minowa MT, Yoshida A, Takeuchi M, Marth JD (2005) Dietary and genetic control of glucose transporter 2 glycosylation promotes insulin secretion in suppressing diabetes. *Cell* **123**: 1307-21
46. Oguri S, Yoshida A, Minowa MT, Takeuchi M (2006) Kinetic properties and substrate specificities of two recombinant human N-acetylglucosaminyltransferase-IV isozymes. *Glycoconj J* **23**: 473-80
47. Khoder-Agha F, Sosicka P, Escriva Conde M, Hassinen A, Glumoff T, Olczak M, Kellokumpu S (2019) N-acetylglucosaminyltransferases and nucleotide sugar transporters form multi-enzyme-multi-transporter assemblies in golgi membranes in vivo. *Cell Mol Life Sci*
48. Iversen MB, Reinert LS, Thomsen MK, Bagdonaite I, Nandakumar R, Cheshenko N, Prabakaran T, Vakhrushev SY, Krzyzowska M, Kratholm SK*, et al.* (2016) An innate antiviral pathway acting before interferons at epithelial surfaces. *Nature immunology* **17**: 150-8
49. Farnsworth A, Wisner TW, Webb M, Roller R, Cohen G, Eisenberg R, Johnson DC (2007) Herpes simplex virus glycoproteins gB and gH function in fusion between the virion envelope and the outer nuclear membrane. *Proc Natl Acad Sci U S A* **104**: 10187-92
50. Bagdonaite I, Norden R, Joshi HJ, King SL, Vakhrushev SY, Olofsson S, Wandall HH (2016) Global Mapping of O-Glycosylation of Varicella Zoster Virus, Human Cytomegalovirus, and Epstein-Barr Virus. *J Biol Chem* **291**: 12014-28
51. Lin E, Spear PG (2007) Random linker-insertion mutagenesis to identify functional domains of herpes simplex virus type 1 glycoprotein B. *Proc Natl Acad Sci U S A* **104**: 13140-5
52. Cooper RS, Heldwein EE (2015) Herpesvirus gB: A Finely Tuned Fusion Machine. *Viruses* **7**: 6552-69
53. Fan Q, Kopp SJ, Byskosh NC, Connolly SA, Longnecker R (2018) Natural Selection of Glycoprotein B Mutations That Rescue the Small-Plaque Phenotype of a Fusion-Impaired Herpes Simplex Virus Mutant. *mBio* **9**
54. Cooper RS, Georgieva ER, Borbat PP, Freed JH, Heldwein EE (2018) Structural basis for membrane anchoring and fusion regulation of the herpes simplex virus fusogen gB. *Nat Struct Mol Biol* **25**: 416-424
55. Delguste M, Peerboom N, Le Brun G, Trybala E, Olofsson S, Bergstrom T, Alsteens D, Bally M (2019) Regulatory Mechanisms of the Mucin-Like Region on Herpes Simplex Virus during Cellular Attachment. *ACS Chem Biol*
56. Delguste M, Zeippen C, Machiels B, Mast J, Gillet L, Alsteens D (2018) Multivalent binding of herpesvirus to living cells is tightly regulated during infection. *Science advances* **4**: eaat1273

57. Mårdberg K, Trybala E, Tufaro F, Bergström T (2002) Herpes simplex virus type 1 glycoprotein C is necessary for efficient infection of chondroitin sulfate-expressing gro2C cells. *J Gen Virol* **83**: 291-300
58. Abidine Y, Liu L, Wallén O, Trybala E, Olofsson S, Bergström T, Bally M (2022) Cellular Chondroitin Sulfate and the Mucin-like Domain of Viral Glycoprotein C Promote Diffusion of Herpes Simplex Virus 1 While Heparan Sulfate Restricts Mobility. *Viruses* **14**
59. Gianni T, Gatta V, Campadelli-Fiume G (2010) {alpha}V{beta}3-integrin routes herpes simplex virus to an entry pathway dependent on cholesterol-rich lipid rafts and dynamin2. *Proc Natl Acad Sci U S A* **107**: 22260-5
60. Nicola AV, Hou J, Major EO, Straus SE (2005) Herpes simplex virus type 1 enters human epidermal keratinocytes, but not neurons, via a pH-dependent endocytic pathway. *J Virol* **79**: 7609-16
61. Rahn E, Petermann P, Hsu MJ, Rixon FJ, Knebel-Mörsdorf D (2011) Entry pathways of herpes simplex virus type 1 into human keratinocytes are dynamin- and cholesterol-dependent. *PLoS One* **6**: e25464
62. Vitiello G, Falanga A, Petruk AA, Merlino A, Fragneto G, Paduano L, Galdiero S, D'Errico G (2015) Fusion of raft-like lipid bilayers operated by a membranotropic domain of the HSV-type I glycoprotein gH occurs through a cholesterol-dependent mechanism. *Soft Matter* **11**: 3003-16
63. Gianni T, Campadelli-Fiume G (2012) αVβ3-integrin relocalizes nectin1 and routes herpes simplex virus to lipid rafts. *J Virol* **86**: 2850-5
64. Loret S, Guay G, Lippé R (2008) Comprehensive characterization of extracellular herpes simplex virus type 1 virions. *J Virol* **82**: 8605-18
65. Marsden HS, Crombie IK, Subak-Sharpe JH (1976) Control of protein synthesis in herpesvirus-infected cells: analysis of the polypeptides induced by wild type and sixteen temperature-sensitive mutants of HSV strain 17. *J Gen Virol* **31**: 347-72
66. Guenalp A (1965) GROWTH AND CYTOPATHIC EFFECT OF RUBELLA VIRUS IN A LINE OF GREEN MONKEY KIDNEY CELLS. *Proc Soc Exp Biol Med* **118**: 85-90
67. Desai P, Person S (1998) Incorporation of the green fluorescent protein into the herpes simplex virus type 1 capsid. *J Virol* **72**: 7563-8
68. Narimatsu Y, Joshi HJ, Yang Z, Gomes C, Chen YH, Lorenzetti FC, Furukawa S, Schjoldager KT, Hansen L, Clausen H*, et al.* (2018) A validated gRNA library for CRISPR/Cas9 targeting of the human glycosyltransferase genome. *Glycobiology* **28**: 295-305
69. Doench JG, Fusi N, Sullender M, Hegde M, Vaimberg EW, Donovan KF, Smith I, Tothova Z, Wilen C, Orchard R*, et al.* (2016) Optimized sgRNA design to maximize activity and minimize off-target effects of CRISPR-Cas9. *Nat Biotechnol* **34**: 184-191
70. Ran FA, Hsu PD, Wright J, Agarwala V, Scott DA, Zhang F (2013) Genome engineering using the CRISPR-Cas9 system. *Nat Protoc* **8**: 2281-2308
71. Sanjana NE SO, Zhang F. (2014) Improved vectors and genome-wide libraries for CRISPR screening. *Nat Methods* **11**: 783-784
72. Ehrhardt C, Schmolke M, Matzke A, Knoblauch A, Will C, Wixler V, Ludwig S (2006) Polyethylenimine, a cost-effective transfection reagent. *Signal transduction Banner* **6**: 179-184
73. Yang Z, Steentoft C, Hauge C, Hansen L, Thomsen AL, Niola F, Vester-Christensen MB, Frodin M, Clausen H, Wandall HH*, et al.* (2015) Fast and sensitive detection of indels induced by precise gene targeting. *Nucleic acids research* **43**: e59

74. Kudelka MR, Antonopoulos A, Wang Y, Duong DM, Song X, Seyfried NT, Dell A, Haslam SM, Cummings RD, Ju T (2016) Cellular O-Glycome Reporter/Amplification to explore O-glycans of living cells. *Nat Methods* **13**: 81-6
75. Yang Z, Wang S, Halim A, Schulz MA, Frodin M, Rahman SH, Vester-Christensen MB, Behrens C, Kristensen C, Vakhrushev SY*, et al.* (2015) Engineered CHO cells for production of diverse, homogeneous glycoproteins. *Nat Biotechnol* **33**: 842-4
76. Dabelsteen S, Hercule P, Barron P, Rice M, Dorsainville G, Rheinwald JG (2009) Epithelial cells derived from human embryonic stem cells display p16INK4A senescence, hypermotility, and differentiation properties shared by many P63+ somatic cell types. *Stem cells (Dayton, Ohio)* **27**: 1388-99
77. Visalli RJ, Courtney RJ, Meyers C (1997) Infection and replication of herpes simplex virus type 1 in an organotypic epithelial culture system. *Virology* **230**: 236-43
78. Namvar L, Olofsson S, Bergstrom T, Lindh M (2005) Detection and typing of Herpes Simplex virus (HSV) in mucocutaneous samples by TaqMan PCR targeting a gB segment homologous for HSV types 1 and 2. *J Clin Microbiol* **43**: 2058-64
79. Sayers CL, Elliott G (2016) Herpes Simplex Virus 1 Enters Human Keratinocytes by a Nectin-1-Dependent, Rapid Plasma Membrane Fusion Pathway That Functions at Low Temperature. *J Virol* **90**: 10379-10389

Figure legends

Figure 1. Human keratinocyte library for probing host-pathogen interplay. A Common cell surface glycoconjugates are depicted, with investigated classes of glycans highlighted in bold and in boxes below. The glycoengineered cell library was generated by knocking out genes involved in respective biosynthetic pathways using CRISPR/Cas9 and ZFN technologies. **B** N-glycoprofiling of cell lines harboring alterations in N-glycan synthesis. **C** O-glyprofiling of cell lines harboring alterations in O-glycan synthesis. **D-F** The array of cell lines was infected with MOI 10 of HSV-1 Syn17+, and viral titers (**D**) and viral DNA content (**E**) in the media were measured at 17 hpi. Particle to PFU ratio is also shown (**F**). Data is shown as WT-normalized mean +SEM of 3 independent experiments for each knock out (KO) cell line. One sample t test was used to evaluate differences from 1 (* $p < 0.05$, ** $p < 0.01$, *** $p < 0.001$, **** $p < 0.0001$).

Figure 2. Binding and entry of HSV-1 to mutant cell lines. A-C 200 PFU of HSV-1 Syn17+ were allowed to adsorb to KO cell line monolayers for 20 min (**A**) or 120 min (**B**) on ice. Resulting plaques were quantified 48 h later. Data is shown as WT-normalized mean +SEM of 3 independent experiments for each KO cell line. One sample t test was used to evaluate differences from 1 (* $p < 0.05$, ** $p < 0.01$, *** $p < 0.001$, **** $p < 0.0001$). **C** Proportion of virus bound at 20 min compared to 120 min is shown as mean +SEM of 3 independent experiments for each KO cell line. One-way ANOVA followed by Dunnett's multiple comparison test was used to evaluate differences from WT (* $p < 0.05$, ** $p < 0.01$, *** $p < 0.001$, **** $p < 0.0001$). **D-E** 200 PFU of HSV-1 Syn17+ were allowed to adsorb to KO cell line monolayers for 120 min on ice followed by 5 min warming to 37 °C and subsequent acid inactivation. Resulting plaques were quantified 48 h later. **D** Data is shown as WT-normalized mean +SEM of 3 independent experiments for each KO cell line. One sample t test was used to evaluate differences from 1 (* $p < 0.05$, ** $p < 0.01$, *** $p < 0.001$, **** $p < 0.0001$). **E** Proportion of virus entered at 5 min compared to virus bound at 120 min is shown as

mean +SEM of 3 independent experiments for each KO cell line. One-way ANOVA followed by Dunnett's multiple comparison test was used to evaluate differences from WT (* $p < 0.05$, ** $p < 0.01$, *** $p < 0.001$, **** $p < 0.0001$). **F** HaCaT WT and *B4GALT7* KO cells were probed for HSV-1 gC binding followed by mouse anti-gC and secondary antibodies. Heparinase 1, 2, and 3, chondroitinase ABC and combined treatments were included to evaluate contributions of HS and CS GAG chains. **G** The cartoon depicts a simplified overview of GAG synthesis. **H** A panel of CHO KO cell lines was used to measure HSV-1 gC binding followed by mouse anti-gC and secondary antibodies by flow cytometry. Control stainings omitted the gC probe and were used for subtracting background. Data is shown as WT-normalized geometrical mean +SEM of 3 independent experiments for each KO cell line. One sample t test was used to evaluate differences from 1 (* $p < 0.05$, ** $p < 0.01$, *** $p < 0.001$, **** $p < 0.0001$).

Figure 3. Viral assembly and properties of glycoengineered virions. A HaCaT cells grown on cover slips were infected with MOI10 of HSV-1 K26-GFP and fixed and permeabilized at 14 hpi followed by co-staining for HSV-1 gD (magenta) and E-cadherin (cyan). Histograms on the left indicate intensities of gD and E-cadherin signals across the confocal images (marked with black arrowheads). Pixel overlap from the two channels is shown in white. GFP labelled capsid proteins (VP26) are seen in green. Nuclei were stained with DAPI (blue). Stainings of mock-infected cells are included. Scale bar: 10 µm. Images are representative of 2 independent experiments. **B** HaCaT cells grown on cover slips were infected with MOI10 of HSV-1 K26-GFP and fixed and permeabilized at 14 hpi followed by staining for HSV-1 gB (magenta). GFP labelled capsid proteins (VP26) are seen in green. Nuclei were stained with DAPI (blue). Scale bar: 10 µm. Magnified regions of merged images are indicated with dashed white boxes. Images are representative of 2 independent experiments. **C** HaCaT WT and *C1GALT1C1* KO cells were infected with MOI3 or MOI10 of HSV-1 K26-GFP and viral capsids imaged by live microscopy at 14 and 20 hpi. Fluorescent images overlaid with bright field images are also shown. **D-F** 200 PFU of HSV-1 Syn17+ produced in the different KO cell lines were allowed to adsorb to HaCaT WT monolayers for 20 min (**D**) or 120 min (**E**) on ice. Resulting plaques were quantified 48 h later. Data is shown as WT-normalized mean +SEM of 3 independent experiments for each glycoengineered virus species. One sample t test was used to evaluate differences from 1 (* $p < 0.05$, ** $p < 0.01$, *** $p < 0.001$, **** $p < 0.0001$). **F** Proportion of virus bound at 20 min compared to 120 min is shown as mean +SEM of 3 independent experiments for each glycoengineered virus species. One-way ANOVA followed by Dunnett's multiple comparison test was used to evaluate differences from WT (* $p < 0.05$, ** $p < 0.01$, *** $p < 0.001$, **** $p < 0.0001$). **G-H** 200 PFU of HSV-1 Syn17+ produced in the different KO cell lines were allowed to adsorb to HaCaT WT monolayers for 120 min on ice followed by 5 min warming to 37 °C and subsequent acid inactivation. Resulting plaques were quantified 48 h later. **G** Data is shown as WT-normalized mean +SEM of 3 independent experiments for each glycoengineered virus species. One sample t test was used to evaluate differences from 1 (* $p < 0.05$, ** $p < 0.01$, *** $p < 0.001$, **** $p < 0.0001$). **H** Proportion of virus entered at 5 min compared to virus bound at 120 min is shown as mean +SEM of 3 independent experiments for each glycoengineered virus species. One-way ANOVA followed by Dunnett's multiple comparison test was used to evaluate differences from WT (* $p < 0.05$, ** $p < 0.01$, *** $p < 0.001$, **** $p < 0.0001$).

Figure 4. Single O-glycosites affect cell-cell fusion efficiency. A HSV-1 gB structure (PDB: 2GUM) with select mutated O-glycan acceptor sites indicated within the dashed box. Respective previously identified O-glycans were drawn manually as yellow squares. Domains are numbered in roman numericals according to Heldwein *et al.*, Science 2006. **B** The cartoon illustrates the principle of split luciferase assay. **C** Cell surface expression of gB O-glycosite Thr to Ala mutants evaluated by CELISA using mouse anti-gB antibodies. Data is shown as mean absorbance at 450 nm +SD of three technical replicates and is representative of three independent experiments. **D-E** Cell-cell fusion activity over 240 min using gB O-glycosite Thr to Ala mutants. Data from two independent experiments is shown, where mean normalized luminescence of three technical replicates at each time point is indicated by a dot. Mean values of the two independent experiments are shown as thin lines. Data is normalized to maximum luminescence reading at final time point using WT gB for each experiment. The upper panel shows apparent measurements, whereas the values in the lower panel were adjusted to account for differences in cell surface expression of gB. **D** Data related to gB domain I mutations. **E** Data related to gB domain V mutations. **F** HSV-1 gD structure (PDB: 2C36) with select mutated O-glycan acceptor sites indicated. Positions after removal of signal peptide, often encountered in the literature, are indicated in brackets. Respective previously identified O-glycans were drawn manually as yellow squares. N-terminal region omitted in the crystal structure is drawn as a dashed line. **G** Cell surface expression of gD O-glycosite Thr to Ala mutants evaluated by CELISA using mouse anti-gD antibodies. Data is shown as mean absorbance at 450 nm +SD of three technical replicates and is representative of three independent experiments. **H** Cell-cell fusion activity over 240 min using gD O-glycosite Ser/Thr to Ala mutants. Data from two independent experiments is shown, where mean normalized luminescence of three technical replicates at each time point is indicated by a dot. Mean values of the two independent experiments are shown as thin lines. Data is normalized to maximum luminescence reading at final time point using WT gD for each experiment. The upper panel shows apparent measurements, whereas the values in the lower panel were adjusted to account for differences in cell surface expression of gD.

Figure 5. HSV-1 cell-to-cell spread in mutant cell monolayers and cultured tissues. A Plaque assay was used to evaluate 2D cell-to-cell spread in glycoengineered HaCaT cell monolayers, and organotypic skin model infections were used for inspecting 3D spread. **B** Plaque diameter on cell monolayers infected with HSV-1 Syn17+ at 48 hpi. Data is presented as violin diagrams that include measurements from 3 independent experiments for each KO cell line, with 50 plaques measured for each experiment. Paired WT data includes measurements from 15 independent experiments. The dashed lines within the plots indicate median diameter, whereas the dotted lines indicate the interquartile range. One-way ANOVA followed by Games-Howell's multiple comparison test was used to evaluate differences from WT (* $p < 0.05$, ** $p < 0.01$, *** $p < 0.001$, **** $p < 0.0001$). **C** Cell monolayers grown on large cover slips were infected with 200 PFU of HSV-1 K26-GFP and overlaid with semi-solid media for 48 h followed by fixation and staining for HSV-1 gE (red). GFP labelled capsid proteins (VP26) are seen in green. Confocal images at two different magnifications were taken to illustrate overviews of plaques (upper panels) as wells as gE expression at higher resolution (lower panels). Scale bars for the different magnifications are indicated. **D-G** Fully differentiated 3D skin models built with glycoengineered cells were infected with HSV-1 Syn17+ for 36 h followed by fixation in formalin and embedding in paraffin. **D** The cartoon illustrates the procedure for evaluating HSV-1 spread in organotypic skin tissues. FFPE

tissues were sectioned every 30 µm for 10 consecutive slices containing two sections each, spanning from the center of the tissue outwards in two directions. **E** Consecutive sections were stained with a polyclonal FITC-labelled anti-HSV-1 antibody to visualize virus lesions and whole sections imaged with a microscope slide scanner. An example section series is shown with HSV-1 lesions outlined in purple. **F** Representative lesions were selected from the scanned section series for each KO tissue. **G** Three lesions spanning several sections were identified for each KO tissue and lesion area measured at the centermost section. Data is shown as mean +SEM with individual measurement values indicated as black dots. One-way ANOVA followed by Dunnett's multiple comparison test was used to evaluate differences from WT (* $p < 0.05$, ** $p < 0.01$, *** $p < 0.001$, **** $p < 0.0001$).

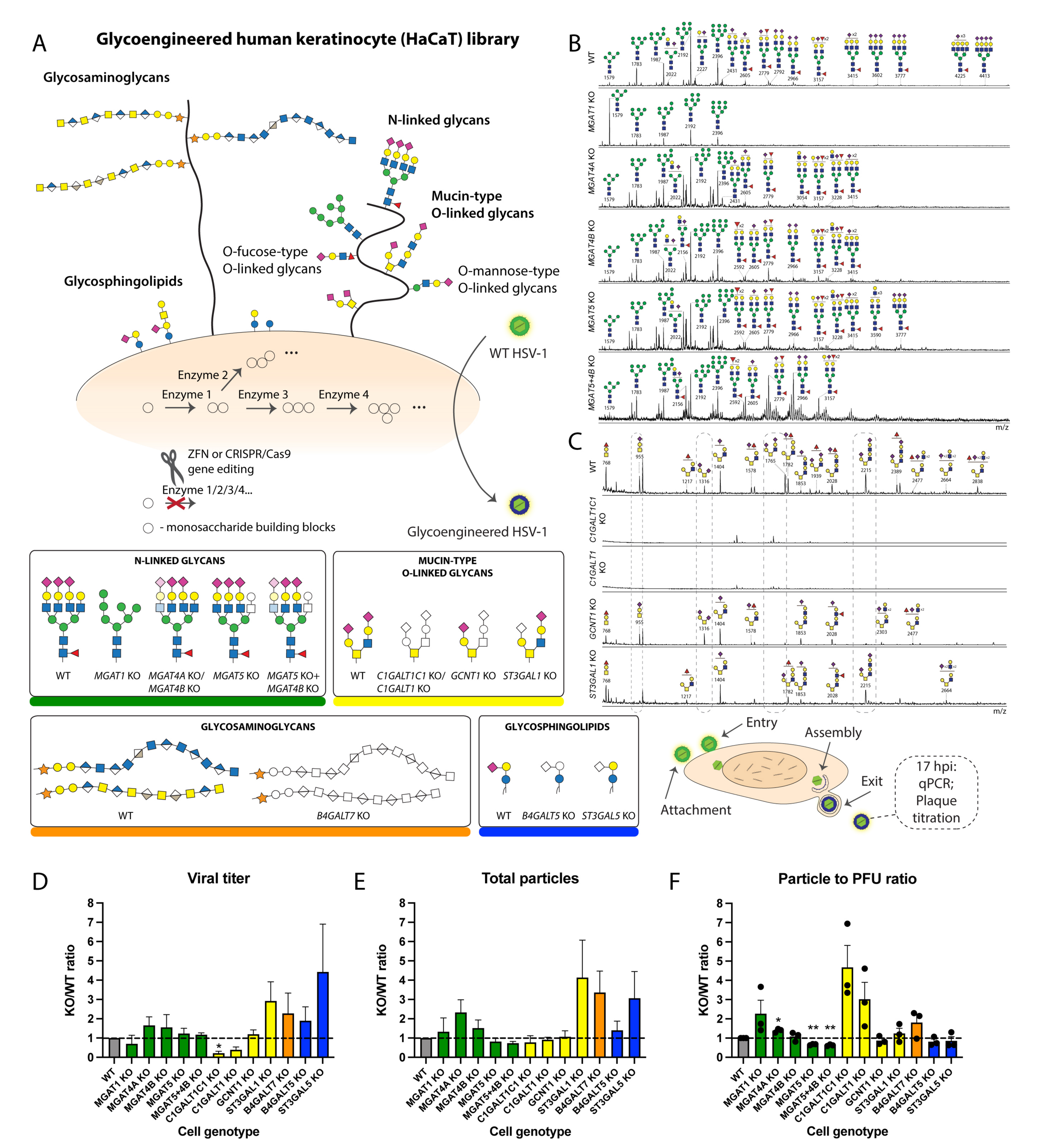
A
Glycoengineered human keratinocyte (HaCaT) library
Glycosaminoglycans
N-linked glycans
Mucin-type O-linked glycans
O-fucose-type O-linked glycans
O-mannose-type O-linked glycans
Glycosphingolipids
WT HSV-1
Enzyme 1
Enzyme 2
Enzyme 3
Enzyme 4
ZFN or CRISPR/Cas9 gene editing
Enzyme 1/2/3/4...
- monosaccharide building blocks
Glycoengineered HSV-1
N-LINKED GLYCANS
WT
MGAT1 KO
MGAT4A KO/ MGAT4B KO
MGAT5 KO
MGAT5 KO+ MGAT4B KO
MUCIN-TYPE O-LINKED GLYCANS
WT
C1GALT1C1 KO/ C1GALT1 KO
GCNT1 KO
ST3GAL1 KO
GLYCOSAMINOGLYCANS
WT
B4GALT7 KO
GLYCOSPHINGOLIPIDS
WT
B4GALT5 KO
ST3GAL5 KO
B
WT
MGAT1 KO
MGAT4A KO
MGAT4B KO
MGAT5 KO
MGAT5+4B KO
m/z
C
WT
C1GALT1C1 KO
C1GALT1 KO
GCNT1 KO
ST3GAL1 KO
m/z
Entry
Assembly
Exit
Attachment
17 hpi: qPCR; Plaque titration
D
Viral titer
KO/WT ratio
Cell genotype
E
Total particles
KO/WT ratio
Cell genotype
F
Particle to PFU ratio
KO/WT ratio
Cell genotype
WT
MGAT1 KO
MGAT4A KO
MGAT4B KO
MGAT5 KO
MGAT5+4B KO
C1GALT1C1 KO
C1GALT1 KO
GCNT1 KO
ST3GAL1 KO
B4GALT7 KO
B4GALT5 KO
ST3GAL5 KO

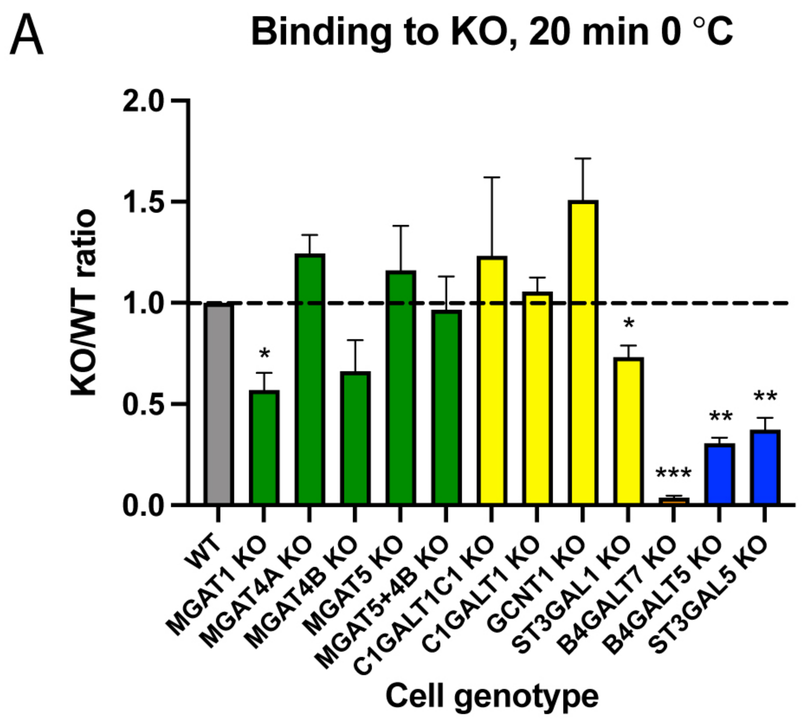
A
Binding to KO, 20 min 0 °C
KO/WT ratio
2.0
1.5
1.0
0.5
0.0
WT
MGAT1 KO
MGAT4A KO
MGAT4B KO
MGAT5 KO
MGAT5+4B KO
C1GALT1C1 KO
C1GALT1 KO
GCNT1 KO
ST3GAL1 KO
B4GALT7 KO
B4GALT5 KO
ST3GAL5 KO
Cell genotype

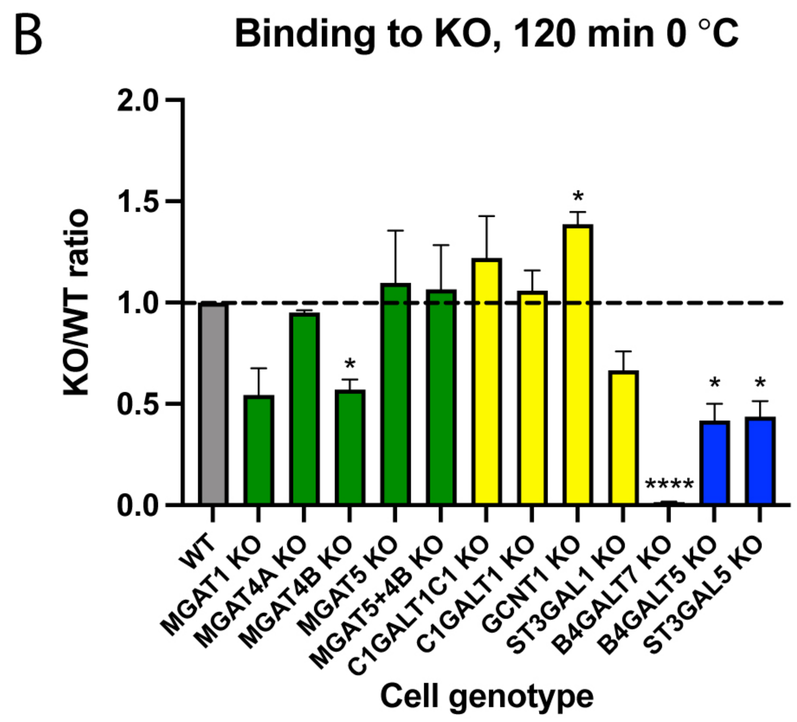
B
Binding to KO, 120 min 0 °C
KO/WT ratio
2.0
1.5
1.0
0.5
0.0
WT
MGAT1 KO
MGAT4A KO
MGAT4B KO
MGAT5 KO
MGAT5+4B KO
C1GALT1C1 KO
C1GALT1 KO
GCNT1 KO
ST3GAL1 KO
B4GALT7 KO
B4GALT5 KO
ST3GAL5 KO
Cell genotype

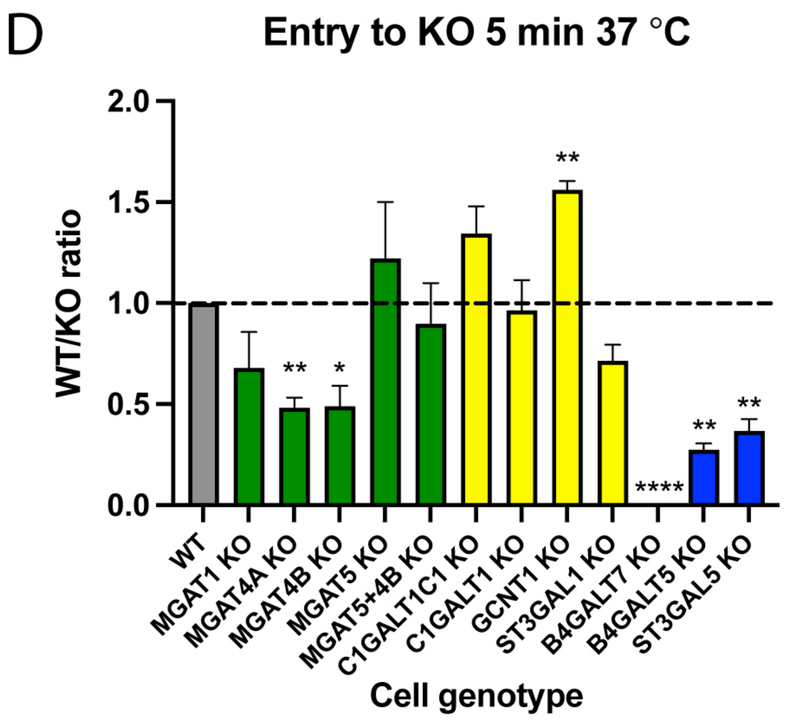
D
Entry to KO 5 min 37 °C
WT/KO ratio
2.0
1.5
1.0
0.5
0.0
WT
MGAT1 KO
MGAT4A KO
MGAT4B KO
MGAT5 KO
MGAT5+4B KO
C1GALT1C1 KO
C1GALT1 KO
GCNT1 KO
ST3GAL1 KO
B4GALT7 KO
B4GALT5 KO
ST3GAL5 KO
Cell genotype

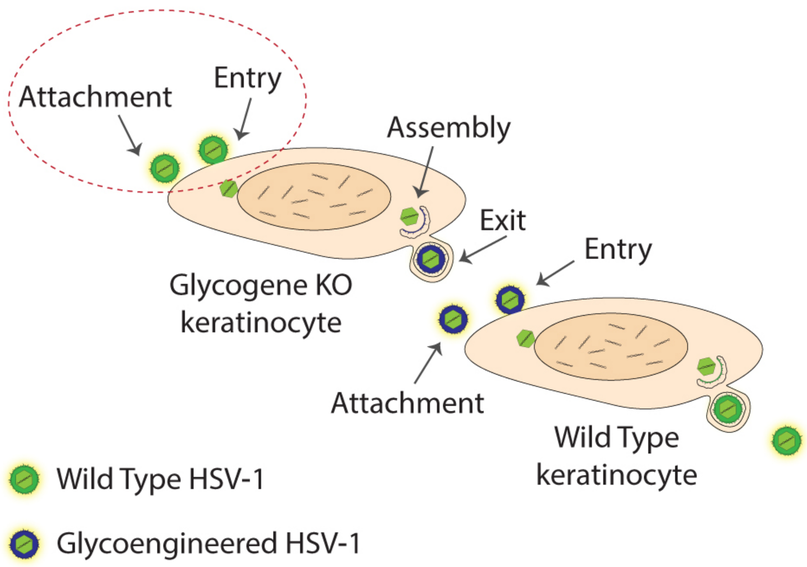
Attachment
Entry
Assembly
Exit
Entry
Glycogene KO
keratinocyte
Attachment
Wild Type
keratinocyte
Wild Type HSV-1
Glycoengineered HSV-1

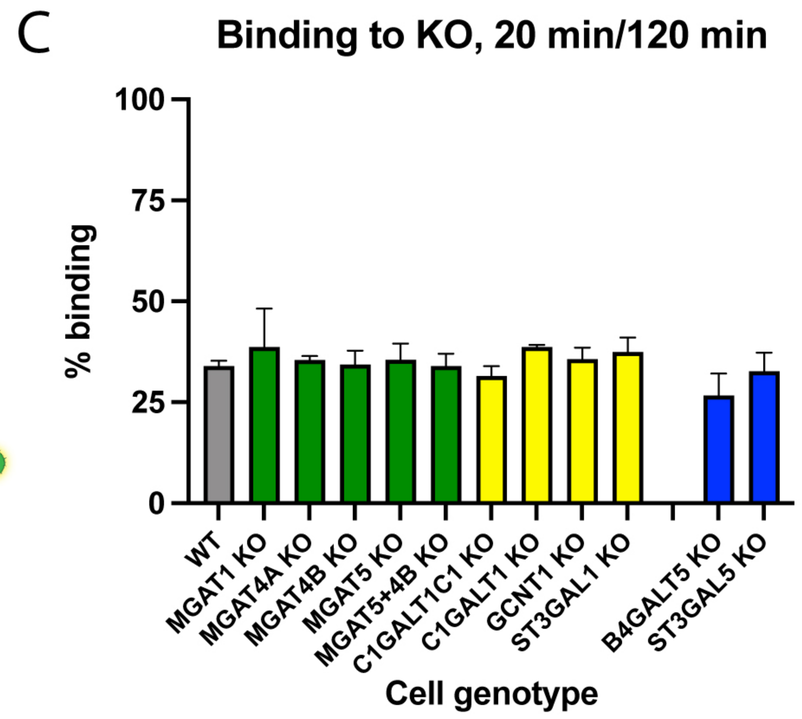
C
Binding to KO, 20 min/120 min
% binding
100
75
50
25
0
WT
MGAT1 KO
MGAT4A KO
MGAT4B KO
MGAT5 KO
MGAT5+4B KO
C1GALT1C1 KO
C1GALT1 KO
GCNT1 KO
ST3GAL1 KO
B4GALT5 KO
ST3GAL5 KO
Cell genotype

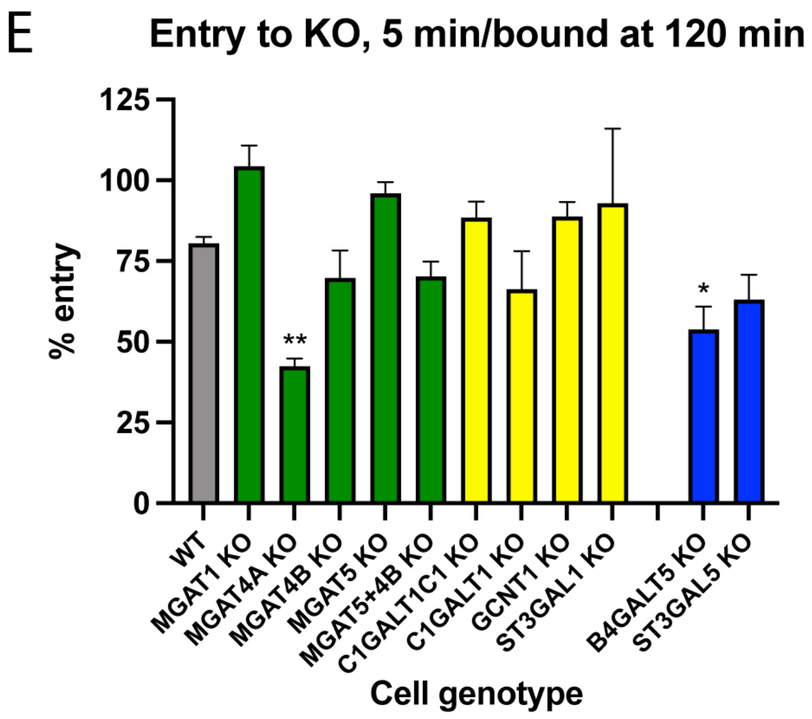
E
Entry to KO, 5 min/bound at 120 min
% entry
125
100
75
50
25
0
WT
MGAT1 KO
MGAT4A KO
MGAT4B KO
MGAT5 KO
MGAT5+4B KO
C1GALT1C1 KO
C1GALT1 KO
GCNT1 KO
ST3GAL1 KO
B4GALT5 KO
ST3GAL5 KO
Cell genotype

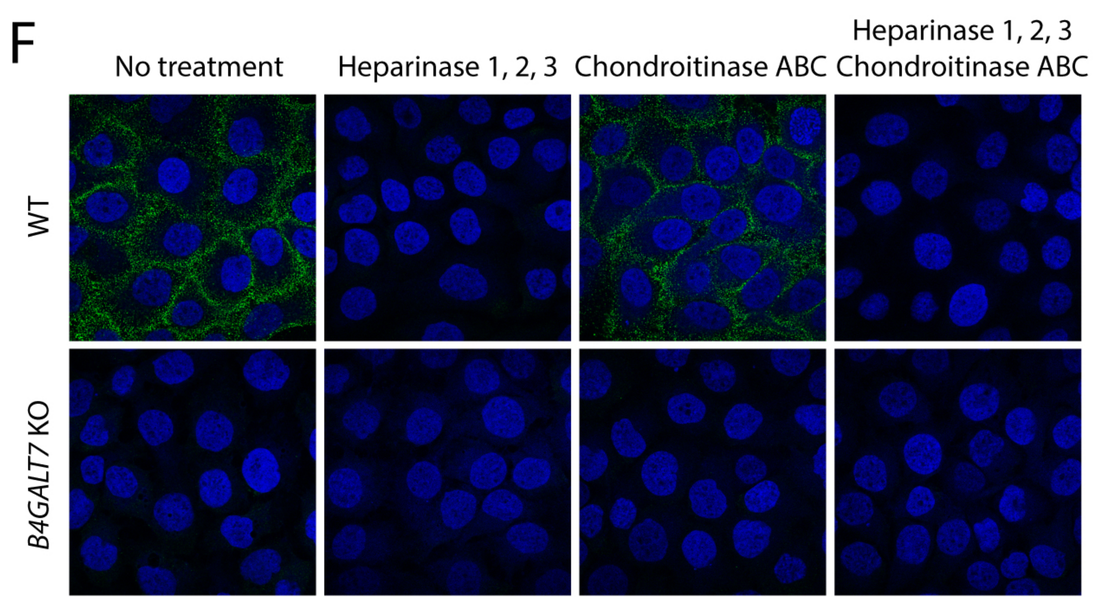
F
No treatment
Heparinase 1, 2, 3
Chondroitinase ABC
Heparinase 1, 2, 3
Chondroitinase ABC
WT
B4GALT7 KO

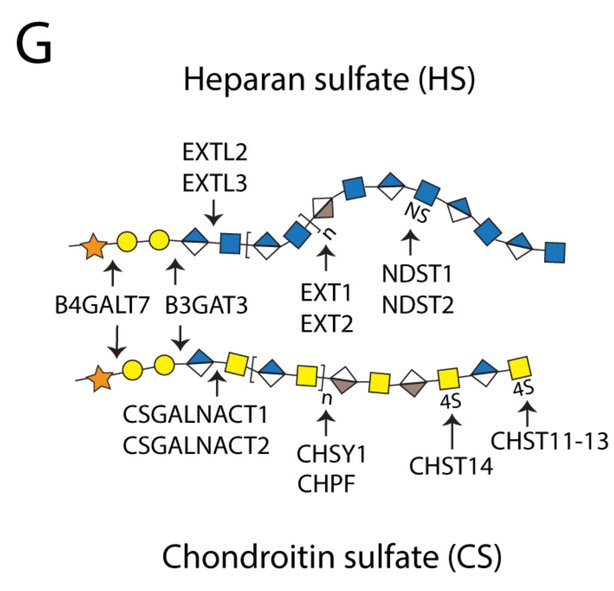
G
Heparan sulfate (HS)
EXTL2
EXTL3
B4GALT7
B3GAT3
EXT1
EXT2
NDST1
NDST2
NS
CSGALNACT1
CSGALNACT2
CHSY1
CHPF
4S
CHST14
CHST11-13
Chondroitin sulfate (CS)

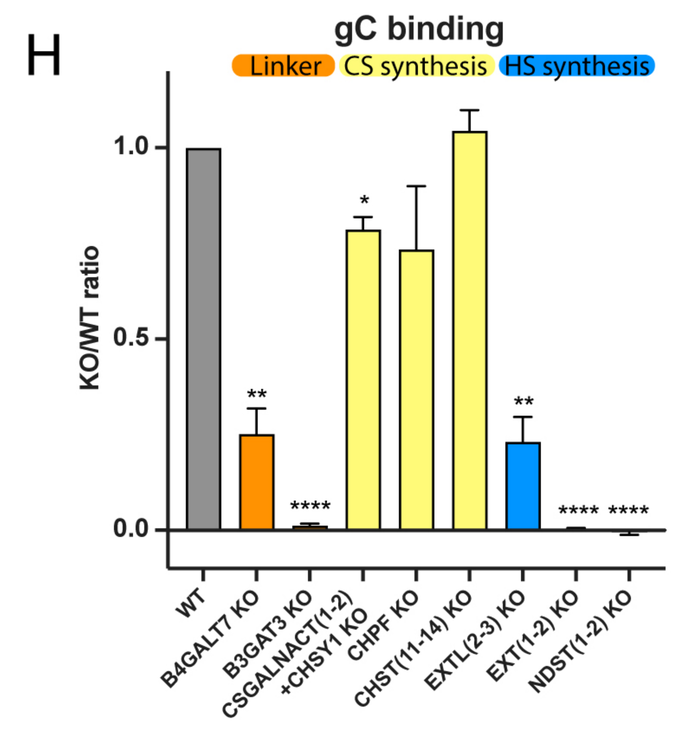
H
gC binding
Linker
CS synthesis
HS synthesis
KO/WT ratio
1.0
0.5
0.0
WT
B4GALT7 KO
B3GAT3 KO
CSGALNACT(1-2)
+CHSY1 KO
CHPF KO
CHST(11-14) KO
EXTL(2-3) KO
EXT(1-2) KO
NDST(1-2) KO

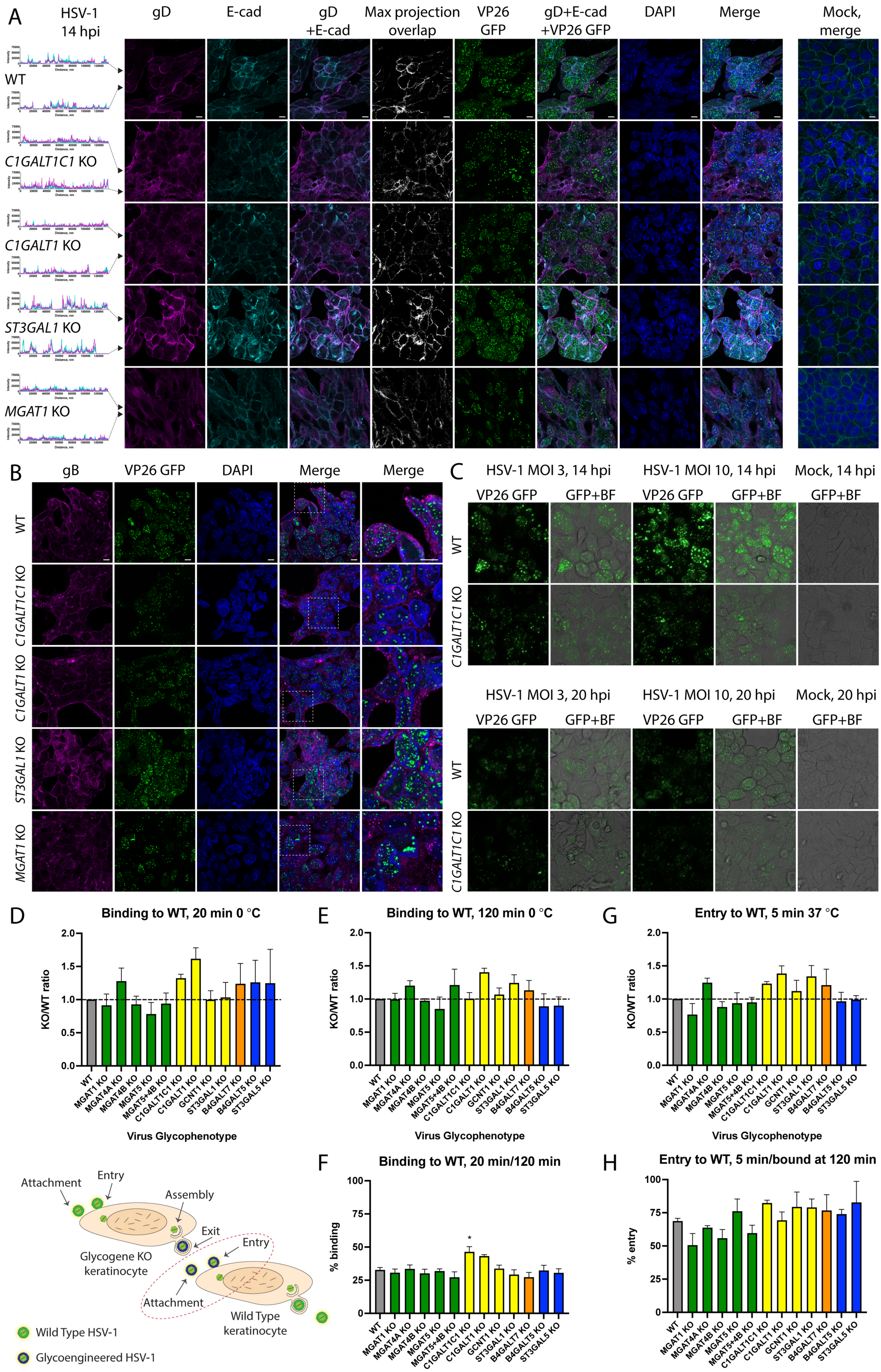
A
HSV-1 14 hpi
gD
E-cad
gD +E-cad
Max projection overlap
VP26 GFP
gD+E-cad +VP26 GFP
DAPI
Merge
Mock, merge
WT
C1GALT1C1 KO
C1GALT1 KO
ST3GAL1 KO
MGAT1 KO
B
gB
VP26 GFP
DAPI
Merge
Merge
C
HSV-1 MOI 3, 14 hpi
HSV-1 MOI 10, 14 hpi
Mock, 14 hpi
VP26 GFP
GFP+BF
HSV-1 MOI 3, 20 hpi
HSV-1 MOI 10, 20 hpi
Mock, 20 hpi
D
Binding to WT, 20 min 0 °C
E
Binding to WT, 120 min 0 °C
G
Entry to WT, 5 min 37 °C
KO/WT ratio
Virus Glycophenotype
Attachment
Entry
Assembly
Exit
Glycogene KO keratinocyte
Wild Type keratinocyte
Wild Type HSV-1
Glycoengineered HSV-1
F
Binding to WT, 20 min/120 min
% binding
H
Entry to WT, 5 min/bound at 120 min
% entry

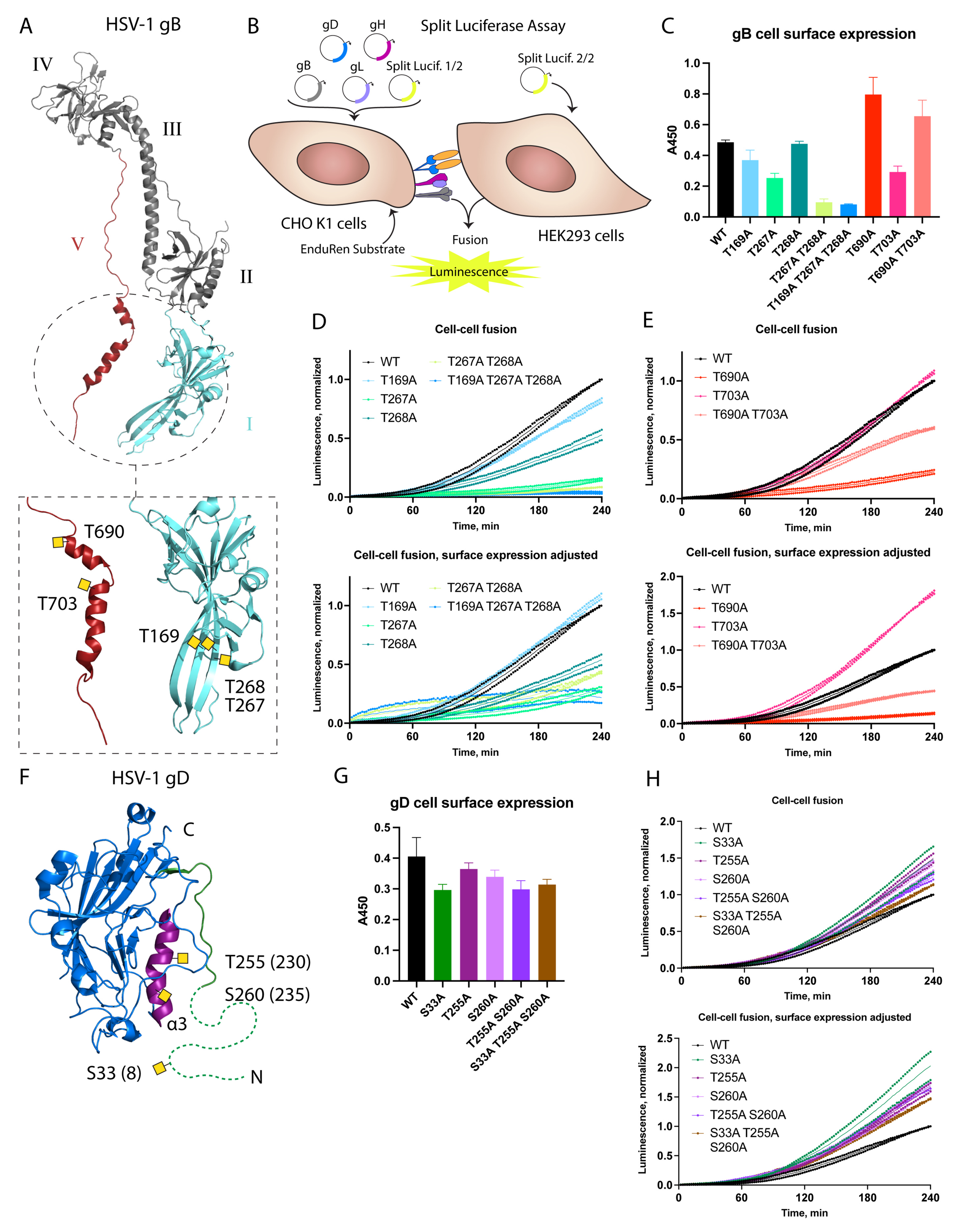
A
HSV-1 gB
IV
III
V
II
I
T690
T703
T169
T268
T267
B
Split Luciferase Assay
gD
gH
gB
gL
Split Lucif. 1/2
Split Lucif. 2/2
CHO K1 cells
EnduRen Substrate
Fusion
HEK293 cells
Luminescence
C
gB cell surface expression
A450
WT
T169A
T267A
T268A
T267A T268A
T169A T267A T268A
T690A
T703A
T690A T703A
D
Cell-cell fusion
Luminescence, normalized
Time, min
Cell-cell fusion, surface expression adjusted
E
Cell-cell fusion
Cell-cell fusion, surface expression adjusted
F
HSV-1 gD
C
T255 (230)
S260 (235)
α3
S33 (8)
N
G
gD cell surface expression
A450
WT
S33A
T255A
S260A
T255A S260A
S33A T255A S260A
H
Cell-cell fusion
Cell-cell fusion, surface expression adjusted
Time, min

A

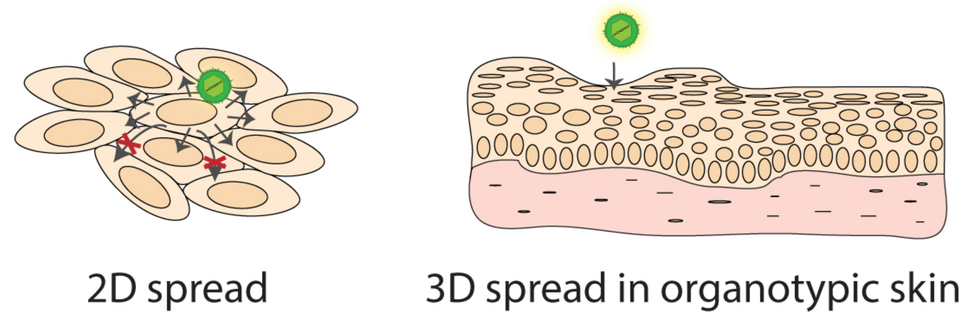
2D spread
3D spread in organotypic skin

B

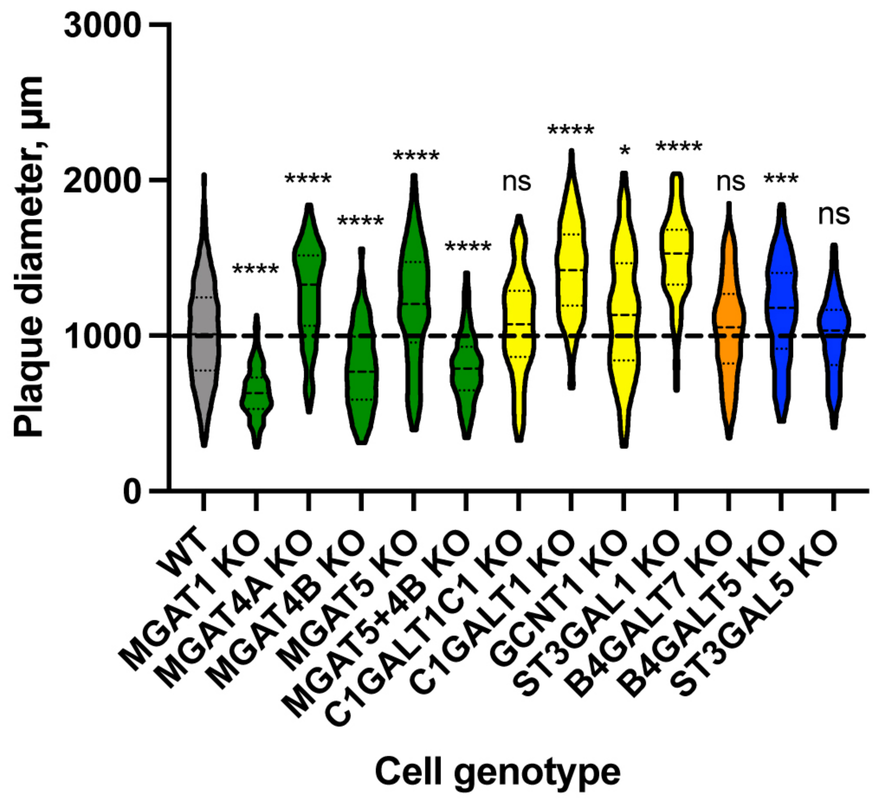
Plaque size distribution
Plaque diameter, µm
3000
2000
1000
0
****
****
****
****
****
ns
****
*
****
ns
***
ns
WT
MGAT1 KO
MGAT4A KO
MGAT4B KO
MGAT5 KO
MGAT5+4B KO
C1GALT1C1 KO
C1GALT1 KO
GCNT1 KO
ST3GAL1 KO
B4GALT7 KO
B4GALT5 KO
ST3GAL5 KO
Cell genotype

C

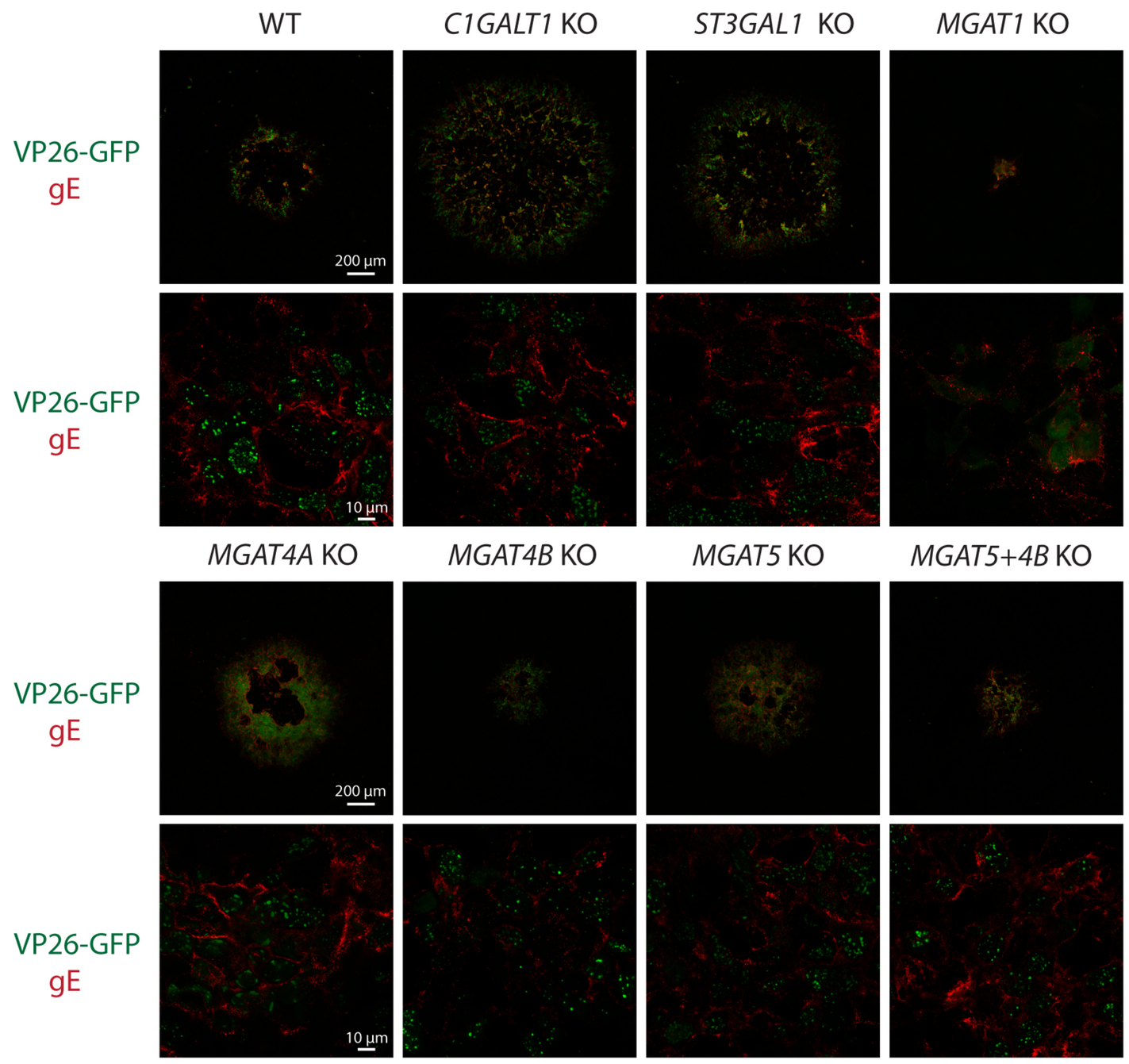
WT
C1GALT1 KO
ST3GAL1 KO
MGAT1 KO
VP26-GFP
gE
200 µm
10 µm
MGAT4A KO
MGAT4B KO
MGAT5 KO
MGAT5+4B KO

D

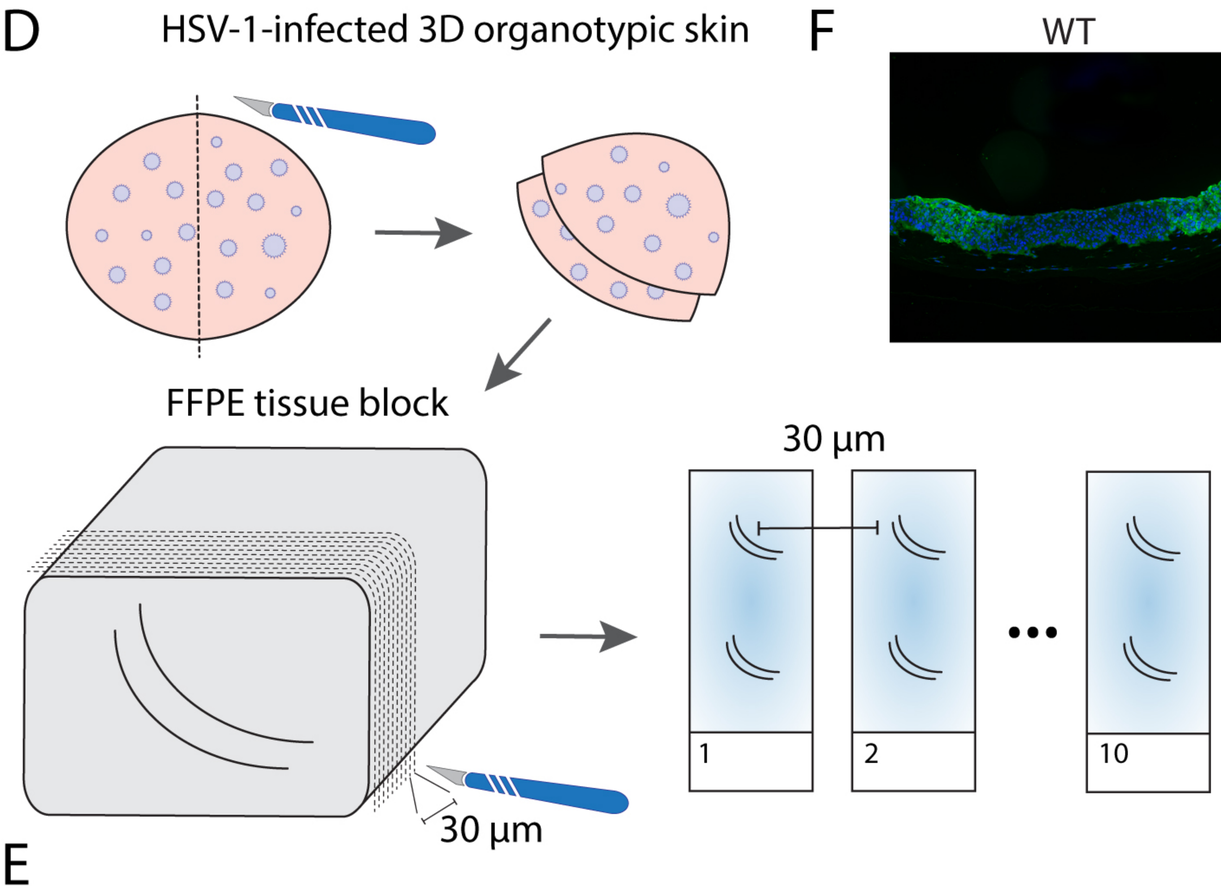
HSV-1-infected 3D organotypic skin
FFPE tissue block
30 µm
1
2
10
30 µm

E

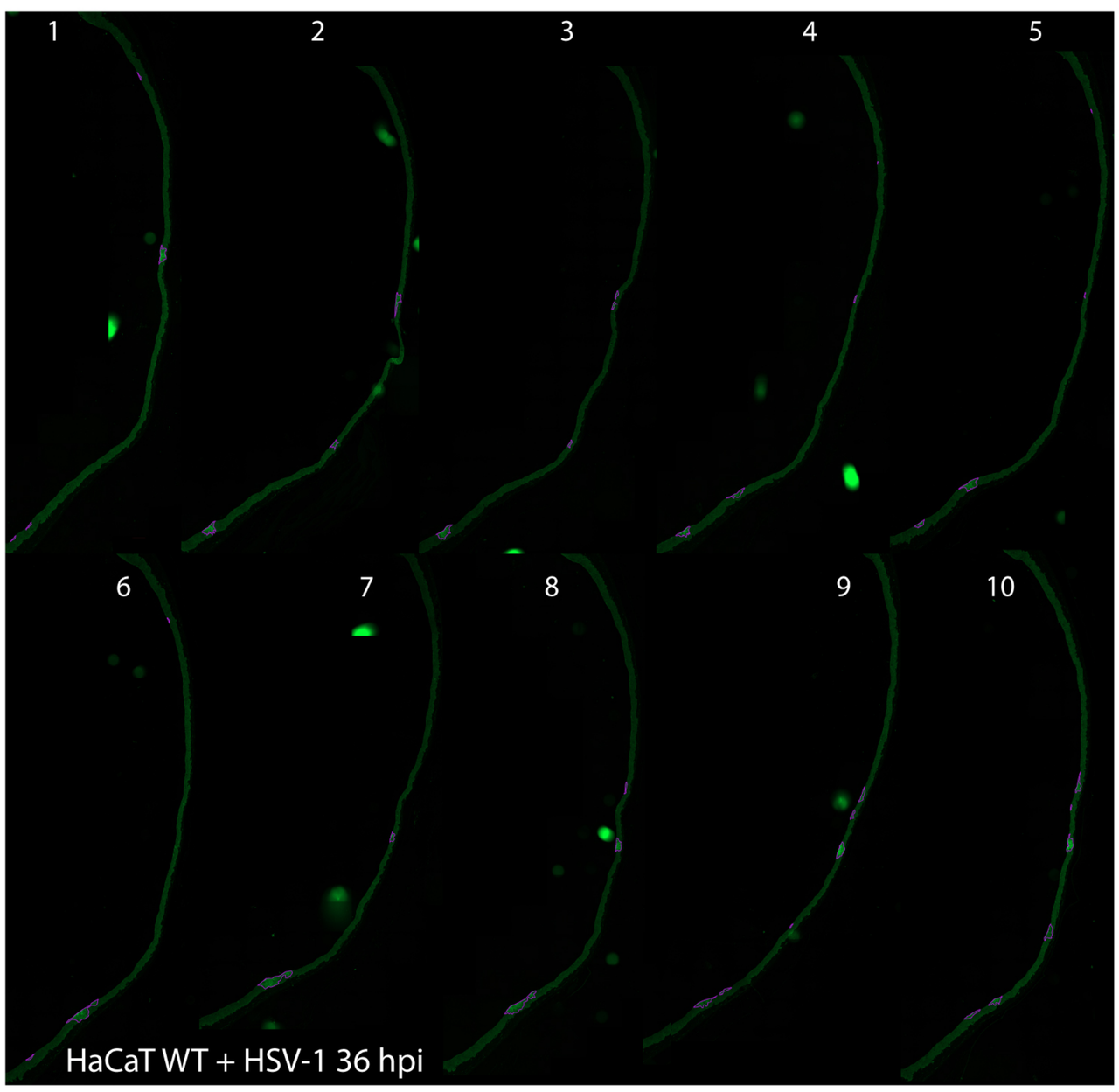
1
2
3
4
5
6
7
8
9
10
HaCaT WT + HSV-1 36 hpi

F

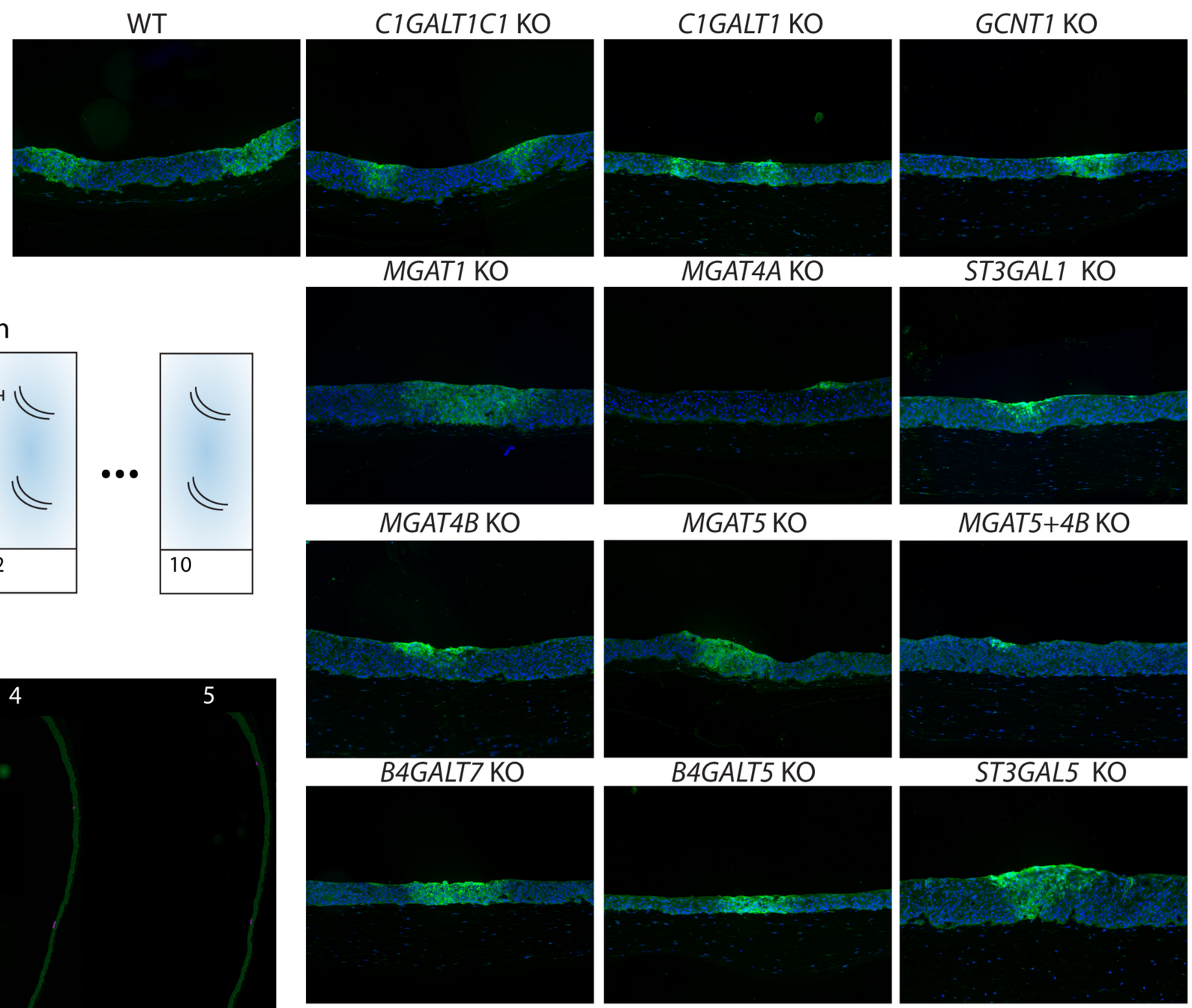
WT
C1GALT1C1 KO
C1GALT1 KO
GCNT1 KO
MGAT1 KO
MGAT4A KO
ST3GAL1 KO
MGAT4B KO
MGAT5 KO
MGAT5+4B KO
B4GALT7 KO
B4GALT5 KO
ST3GAL5 KO

G

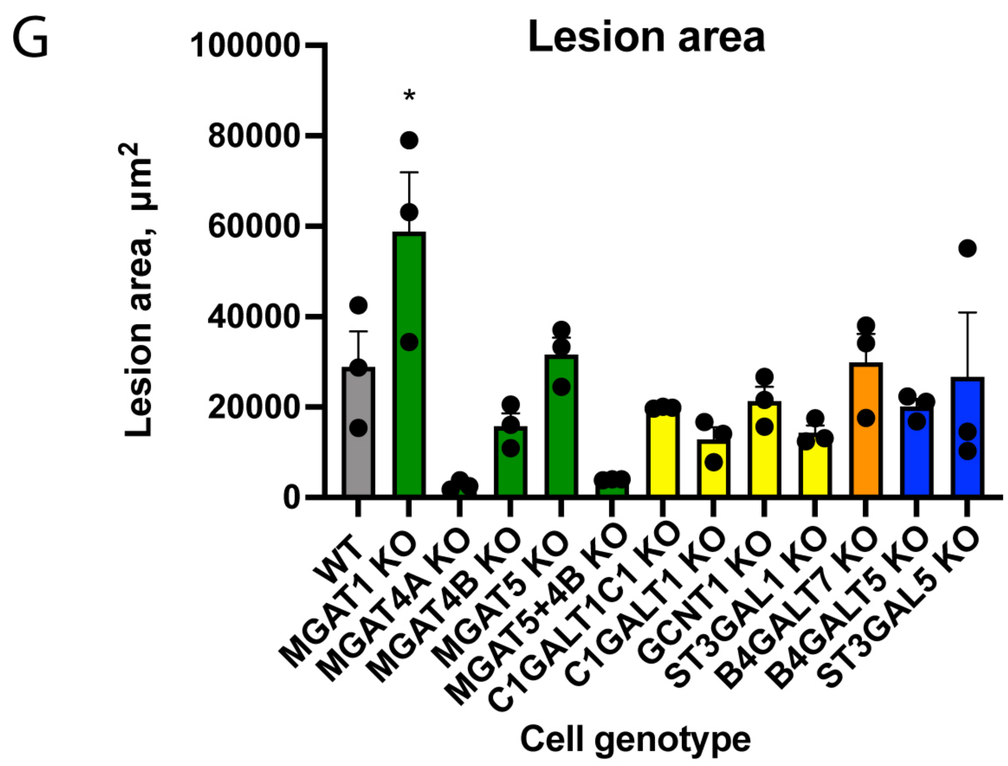
Lesion area
Lesion area, µm²
100000
80000
60000
40000
20000
0
*
WT
MGAT1 KO
MGAT4A KO
MGAT4B KO
MGAT5 KO
MGAT5+4B KO
C1GALT1C1 KO
C1GALT1 KO
GCNT1 KO
ST3GAL1 KO
B4GALT7 KO
B4GALT5 KO
ST3GAL5 KO
Cell genotype

Table S1. Knock out indel sequencing and sgRNA/ZFN targeting sequences

Gene	Clone	Sequence[1]	gRNA/ZFN (5'-3')	Indel	First affected a.a.
N-Glycan					
MGAT1 KO	REF	GATtcgcctggcccaagacgccgAGG	TCGCCTGGCCCAAGACGCCG		
	1E7_A1	GATtcgcctggcccaag----cgCGG		-4	60
	1E7_A2	GATtcgcctggcccaagacg-cgAGG		-1	61
MGAT4A KO	REF	aatgagatgaggctccgcaaTGGAAC	AATGAGATGAGGCTCCGCAA		
	3C10_A1	aatgagatgaggctcc--aaTGGAAC		-2	4
	3C10_A2	aatgagatgaggctccgca-TGGAAC		-1	5
MGAT4B KO	REF	TTG…GCAggagagcctcaagc-gctccaAGGAGCTCAACCTGGTGCTGG	GGAGAGCCTCAAGCGCTCCA		
	3F8_A1	TTG…GCAggagagcctcaagcTgctccaAGGAGCTCAACCTGGTGCTGG		+1	60
	3F8_A2	TTG…----------TGG		-96	36
MGAT5+4B KO	2B5 A1 (in M*GAT5* KO 1F12)	TTG…GCAgga----------GAGCTCAACCTGGTGCTGG		-19	56
MGAT5 KO	REF	GGGCCAtac-------gctggagtcatgacagcTTAT	GCTGTCATGACTCCAGCGTA		
	1F12_A1	GGGCCAtacA------gctggagtcatgacagcTTAT		+1	74
	1F12_A2	GGGCCACATGACATAGgctggagtcatgacagcTTAT		+7	73
O-GalNAc					
C1GALT1C1 KO[2]	REF	ATCACCCCAACCAGGTAGTagaaggctGTTGTTCAGATAT	AGAAGGCT (ZFN cut site)		
	D5_A1	ATCACCCCAACCAGGTA----------GTTGTTCAGATAT		-10	267

[1] Sequences are shown in the orientation of the gene, with sgRNA recognition sequences (direct or complementary)/ZFN cut sites in lower case and PAM sequences underlined

[2] Radhakrishnan *et al*., 2014 (DOI: 10.1073/pnas.1406619111)

C1GALT1 KO	REF	GCCCAgcgttgtaacaaagtgttgtTTATGAGTTCAGAA	ACAACACTTTGTTACAACGC		
	2E5_A1	GCCCAG--TTGTAACAAAGTGTTGTTTATGAGTTCAGAA		-2	114
	2E5_A2	GCCCAGCG----------TGTTGTTTATGAGTTCAGAA		-11	115
GCNT1 KO	REF	AATCACCTtctccgttttaaggattcatCAA	ATGAATCCTTAAAACGGAGA		
	2E7_A1	AAT----------ttaaggattcatCAA		-13	27
	2E7_A2	AATCACCTtc--cgttAATGggattcatCAA		-2	30
ST3GAL1 KO	REF	TGGTGCCCttc-aagaccatcgacttggaGTGGG	TCCAAGTCGATGGTCTTGAA		
	2B2_A1	TGGTGCCCttcAaagaccatcgacttggaGTGGG		+1	210
GAG					
B4GALT7 KO	REF	TGCACGACGTtgacctgctccctctcaa-cgAGGAGCTGGAC	TGACCTGCTCCCTCTCAACG		
	3D9_A1	TGCACGACGTtgacctgctccctctcaaAcgAGGAGCTGGAC		+1	170
	3D9_A2	TGCACGACGTtgacctgctccctctc----------AC		-13	170
GSL					
B4GALT5 KO	REF	AGCCTTCTGATTGCat----------gccTCGGTGGAAG	ATGCC (ZFN cut site)		
	D11_A1	AGCCTTCTGATTGCATGTAGAATTCCCTAGCCTCGGTGGAAG		+13	160
ST3GAL5 KO	REF	GTTatttgagcacaggtata-gcgTGGACTTAC	ATTTGAGCACAGGTATAGCG		
	1C5_A1	GTTatttgagcacaggtataCgcgTGGACTTAC		+1	138
	1C5_A2	GTTatttgagcGTAA---------TGGACTTAC		-8	135

Table S2. Sequences of mutagenic primers. Altered nucleotides are shown in red.

Name	5’ to 3’	Length
gB_T169A	GTACTACAAAGACGTCGCCGTTTCGCAGGTGTG	33
gB_T267A	CCACCGGTACGGGGCGACGGTAAACTG	27
gB_T268A	ACCGGTACGGGACGGCGGTAAACTGCATC	29
gB_T267A_T268A	TCCACCGGTACGGGGCGGCGGTAAACTGCATC	32
gB_T690A	CCTGGAGGTGTACGCCCGCCACGAGATC	28
gB_T703A	CCTGCTGGACTACGCGGAGGTCCAGCG	27
gD_S33A	CCTTGGCGGATGCCGCTCTCAAGATGGCC	29
gD_T255A	CGAGAACCAGCGCGCCGTCGCCGTATA	27
gD_S260A	ACCGTCGCCGTATACGCCTTGAAGATCGCCGG	32
gD_T255A_S260A	CGAGAACCAGCGCGCCGTCGCCGTATACGCCTTGAAGATCGCCGG	45

Figure S1. Multiple sequence alignment for the DNA regions corresponding to the positions of introduced single amino acid mutations in HSV-1 gB and gD expression constructs. Asterisks indicate identical nucleotides.

```
gB Tyr165-Val173          TyrLysAspValThrValSerGlnVal
                           Y  K  D  V  T  V  S  Q  V
gB_WT                     TACAAAGACGTCACCGTTTCGCAGGTG   27
gB_T169A                  TACAAAGACGTCGCCGTTTCGCAGGTG   27
gB_T267A                  TACAAAGACGTCACCGTTTCGCAGGTG   27
gB_T268A                  TACAAAGACGTCACCGTTTCGCAGGTG   27
gB_T267A_T268A            TACAAAGACGTCACCGTTTCGCAGGTG   27
gB_T690A                  TACAAAGACGTCACCGTTTCGCAGGTG   27
gB_T703A                  TACAAAGACGTCACCGTTTCGCAGGTG   27
gB_T690A_T703A            TACAAAGACGTCACCGTTTCGCAGGTG   27
gB_T169A_T267A_T268A      TACAAAGACGTCGCCGTTTCGCAGGTG   27
                          ************ **************

gB His263-Ile272          HisArgTyrGlyThrThrValAsnCysIle
                           H  R  Y  G  T  T  V  N  C  I
gB_WT                     CACCGGTACGGGACGACGGTAAACTGCATC   30
gB_T169A                  CACCGGTACGGGACGACGGTAAACTGCATC   30
gB_T267A                  CACCGGTACGGGGCGACGGTAAACTGCATC   30
gB_T268A                  CACCGGTACGGGACGGCGGTAAACTGCATC   30
gB_T267A_T268A            CACCGGTACGGGGCGGCGGTAAACTGCATC   30
gB_T690A                  CACCGGTACGGGACGACGGTAAACTGCATC   30
gB_T703A                  CACCGGTACGGGACGACGGTAAACTGCATC   30
gB_T690A_T703A            CACCGGTACGGGACGACGGTAAACTGCATC   30
gB_T169A_T267A_T268A      CACCGGTACGGGGCGGCGGTAAACTGCATC   30
                          ************ ** **************

gB Glu687-Gln706          GluValTyrThrArgHisGluIleLysAspSerGlyLeuLeuAspTyrThrGluValGln
                           E  V  Y  T  R  H  E  I  K  D  S  G  L  L  D  Y  T  E  V  Q
gB_WT                     GAGGTGTACACCCGCCACGAGATCAAGGACAGCGGCCTGCTGGACTACACGGAGGTCCAG   60
gB_T169A                  GAGGTGTACACCCGCCACGAGATCAAGGACAGCGGCCTGCTGGACTACACGGAGGTCCAG   60
gB_T267A                  GAGGTGTACACCCGCCACGAGATCAAGGACAGCGGCCTGCTGGACTACACGGAGGTCCAG   60
gB_T268A                  GAGGTGTACACCCGCCACGAGATCAAGGACAGCGGCCTGCTGGACTACACGGAGGTCCAG   60
gB_T267A_T268A            GAGGTGTACACCCGCCACGAGATCAAGGACAGCGGCCTGCTGGACTACACGGAGGTCCAG   60
gB_T690A                  GAGGTGTACGCCCGCCACGAGATCAAGGACAGCGGCCTGCTGGACTACACGGAGGTCCAG   60
gB_T703A                  GAGGTGTACACCCGCCACGAGATCAAGGACAGCGGCCTGCTGGACTACGCGGAGGTCCAG   60
gB_T690A_T703A            GAGGTGTACGCCCGCCACGAGATCAAGGACAGCGGCCTGCTGGACTACGCGGAGGTCCAG   60
gB_T169A_T267A_T268A      GAGGTGTACACCCGCCACGAGATCAAGGACAGCGGCCTGCTGGACTACACGGAGGTCCAG   60
                          ********* ************************************** ***********

gD Leu29-Ala37            LeuAlaAspAlaSerLeuLysMetAla
                           L  A  D  A  S  L  K  M  A
gD_WT                     TTGGCGGATGCCTCTCTCAAGATGGCC   27
gD_S33A                   TTGGCGGATGCCGCTCTCAAGATGGCC   27
gD_T255A                  TTGGCGGATGCCTCTCTCAAGATGGCC   27
gD_S260A                  TTGGCGGATGCCTCTCTCAAGATGGCC   27
gD_T255A_S260A            TTGGCGGATGCCTCTCTCAAGATGGCC   27
gD_S33A_T255A_S260A       TTGGCGGATGCCGCTCTCAAGATGGCC   27
                          ************ **************

gD Glu251-Ala264          GluAsnGlnArgThrValAlaValTyrSerLeuLysIleAla
                           E  N  Q  R  T  V  A  V  Y  S  L  K  I  A
gD_WT                     GAGAACCAGCGCACCGTCGCCGTATACAGCTTGAAGATCGCC   42
gD_S33A                   GAGAACCAGCGCACCGTCGCCGTATACAGCTTGAAGATCGCC   42
gD_T255A                  GAGAACCAGCGCGCCGTCGCCGTATACAGCTTGAAGATCGCC   42
gD_S260A                  GAGAACCAGCGCACCGTCGCCGTATACGCCTTGAAGATCGCC   42
gD_T255A_S260A            GAGAACCAGCGCGCCGTCGCCGTATACGCCTTGAAGATCGCC   42
gD_S33A_T255A_S260A       GAGAACCAGCGCGCCGTCGCCGTATACGCCTTGAAGATCGCC   42
                          ************ **************  *************
```